Uncertain Network Dynamics

NOAH WILLIAMS
Miami Herbert Business School, University of Miami

I study the dynamic transmission across a network of shocks with uncertain dynamic properties using tools from robust control theory to measure system performance. I characterize the response of networks to (1) specified stochastic shocks, where performance is measured by output volatility, or (2) uncertain but norm-bounded inputs, where robust performance is worst-case shock amplification. I apply the framework to production networks, showing how dynamic shock amplification depends on network topology, aggregation, and the directionality of input-output linkages. I first develop some analytic examples, then apply the methods to data on the US production network. I find that over time the US economy has become more fragile and subject to volatility coming through the production network. This reflects both the growing concentration of activity in services, real estate, and finance, and the increased importance of these sectors as inputs.

1. INTRODUCTION

Decentralized, networked interactions play an increasingly central role in modern economic systems. From production and supply chains to financial linkages and informational flows, many key aggregate phenomena emerge from interactions across agents or firms with localized or specialized links. As a result, a growing literature studies how network structure shapes aggregate outcomes, and the resilience and fragility of such systems in their response to local disturbances, failures, or shocks.[1] However, most of this literature, with notable exceptions discussed below, focuses on static models and characterizes the long-run cross-sectional impacts of shocks.

By contrast, I study the dynamics of flows on networks, showing how shocks and uncertainty propagate across the network. I consider a continuous-time model in which the system evolves according to a perturbed differential equation on a directed, weighted graph. The network is represented by an asymmetric matrix, capturing both the directionality and heterogeneity of links. The perturbations are inputs to the system, and represent both stochastic shocks and uncertain disturbances such as modeling errors. The resulting system describes diffusion of shocks or perturbations over time and through the network, which I analyze using methods from control theory. In particular, I

Noah Williams: noahwilliams@miami.edu
I thank Ben Golub, Matt Jackson, and Chao Wei for helpful comments and discussion.

[1] The economic literature on networks includes important and comprehensive surveys by Jackson (2008), Pass (2019), and Goyal (2023), which study the formation and economic implications of networked interactions. Each of these books contains detailed references to the literature.

develop a state-space model of perturbed Laplacian dynamics on networks.[2] The main application in this paper is the seminal Long and Plosser (1983) production network model. In Williams (2026), I apply the methods developed here to study disagreement dynamics in information networks.

In the Long and Plosser (1983) model, supplier relationships characterize how shocks to a sector affect downstream sectors. Static or steady-state versions of this model have been widely studied in the networks literature, following Acemoglu, Carvalho, Ozdaglar, and Tahbaz-Salehi (2012). Carvalho and Tahbaz-Salehi (2019) provide a good summary and overview.[3] Although many later applications are static, the original Long and Plosser (1983) model has a dynamic structure utilized in the business cycle literature.[4] Some recent work also analyzes related dynamic production network models.[5] I show that the equilibrium follows a version of Laplacian dynamics.

While I study the impact of shocks in a fixed network, a related literature studies how the network itself may respond to shocks and lead to amplification. This includes work studying how uncertainty and incentives can affect the formation and fragility of networks.[6] Related papers show how shocks can reconfigure network links and generate cascades.[7] Complementary research by Elliott and Jackson (2026) studies how, in an existing network, reallocation following disruptions can amplify short-run responses to shocks. My results can be interpreted as a stress test for networks that are either technologically fixed or generated endogenously in these models.

I map network dynamics into a control system, making use of "Laplace" methods in two important ways. First, the dynamics on the network are governed by a differential equation involving the graph Laplacian, which characterizes how shocks or other inputs diffuse or propagate across the nodes of the network. The Laplacian essentially becomes the state matrix in a control system. Second, I take the Laplace transform of the system, converting time-domain behavior into the frequency domain. This double use of Laplace techniques allows me to reframe the perturbed or stochastic network dynamics as a transfer function which maps inputs to outputs. I then apply methods from

[2] Related Laplacian dynamics are commonly used to study diffusion on networks, as in Newman (2018), Veerman and Lyons (2020), and Van Mieghem (2023).

[3] Other contributions emphasizing the role of input-output networks and sectoral linkages include Baqaee and Farhi (2019), Baqaee and Farhi (2020). Empirical and international applications include Boehm, Flaaen, and Pandalai-Nayar (2019), and Huo, Levchenko, and Pandalai-Nayar (2025).

[4] Important later work includes Horvath (1998), Dupor (1999), Gabaix (2011) and Atalay (2017), who highlight the potential for idiosyncratic shocks to generate aggregate fluctuations. Foerster, Sarte, and Watson (2011) study the implications of a related model for the factor structure of shocks, and vom Lehn and Winberry (2022) add an investment network along with the production network.

[5] In a model close to mine, Liu and Tsyvinski (2024) study a production network with dynamics driven by adjustment costs. Schaal and Taschereau-Dumouchel (2025) study a dynamic production network with heterogeneous time-to-build and also use spectral and frequency-domain methods. Carvalho, Covarrubias, and Nuño (2025) study a nonlinear dynamic network model under uncertainty where the endogenous response of capital amplifies the welfare cost of business cycles.

[6] See, for example, Acemoglu and Azar (2020), Elliott, Golub, and Leduc (2022), and Kopytov, Mishra, Nimark, and Taschereau-Dumouchel (2024).

[7] See Baqaee (2018) and Taschereau-Dumouchel (2025).

control theory to characterize the volatility of network outputs and the robustness or fragility of different network structures.[8]

The control system approach allows for two broad frameworks to study the performance of the network under uncertainty. In the first, I analyze the impact of stochastic shocks on the network output. In this case, the input is a process with specified properties.[9] This naturally leads to measures of network performance which are tied to the variance of the system output, a measure which is known as the $\mathcal{H}_2$ norm. In the frequency domain, this measure averages network performance across frequencies.

But the control system approach also accommodates a broader notion of uncertainty, when the input is an uncertain process potentially correlated with the state vector satisfying a norm bound. This approach, which is common in robust control, covers general exogenous shock processes with unspecified correlations, as well as broader uncertainty about the structure and dynamics of the network itself. Without a specification of the input other than its bound, a worst-case analysis provides a robust bound on the network performance. In the frequency domain, this performance measure considers the worst-case performance across frequencies, a measure which is known as the $\mathcal{H}_\infty$ norm.[10] The worst-case performance analysis reveals how certain combinations of shocks across the network could be very damaging to the system performance.

Throughout, I treat the network structure as fixed, analyzing the properties of a given network subjected to shocks of uncertain structure and timing. In the control-theory terminology, I focus here on analysis not synthesis. The methods I develop allow me to assess both the performance (how well the network transmits or attenuates inputs) and robustness (how sensitive it is to model uncertainty or disturbance variation) of different network structures. These results are useful on their own, and provide inputs for decisions on routing or allocations across the network, as well as analysis of network design and adaptation.

The networks literature has developed centrality measures of the importance of nodes. A large class of such measures arises from spectral or eigenvalue decompositions of the network matrix, which in turn are tied to long-run dynamic properties.[11] I show that for network performance under uncertainty, the singular values of the control system govern how shocks are amplified. The $\mathcal{H}_2$ performance metric can be written as the sum of squared singular values integrated across frequencies, while the $\mathcal{H}_\infty$ norm is the maximal singular value across frequencies. For undirected or normal networks, singular values reduce to the absolute values of eigenvalues, but for general directed networks the singular values differ.

[8] The control-theoretic framework employed here is developed in Zhou, Doyle, and Glover (1996), Zhou and Doyle (1998) and Skogestad and Postlethwaite (2005). Hansen and Sargent (2008) pioneered the development and application of robust control methods in economics.

[9] In the baseline case, the shocks are Gaussian white noise. Correlated shocks can be analyzed by expanding the state space.

[10] Related frequency domain analysis of robustness in economics includes Onatski and Williams (2003), Brock and Durlauf (2005), and Brock, Durlauf, and Rondina (2013).

[11] Eigenvector and Katz-Bonacich centrality, from Katz (1953) and Bonacich (1987), are used in network games following Ballester, Calvó-Armengol, and Zenou (2006), as well as the production network and information diffusion literature discussed above. See Bloch, Jackson, and Tebaldi (2023) for an overview of network centrality measures.

I apply the methods developed here to study the production network in the United States. Using data from the U.S. Bureau of Economic Analysis (2026), I analyze the US production network both cross-sectionally at different levels of aggregation, and across time. I find that most of the sources of volatility and fragility in the detailed industry-level network come from shocks and uncertainty at the sectoral or coarser levels of aggregation. The most damaging shock vector is concentrated in services, real estate, and finance, then propagates to the rest of the economy. Using the panel data, I find that between 1997 and 2023 the US economy became somewhat more fragile and subject to aggregate output volatility coming through the production network. I show that these changes are driven by two main factors: (1) the increased concentration of economic activity in services and real estate, so shocks to these sectors now have a larger direct effect on aggregate output, and (2) the increased importance of finance and real estate as inputs across many different sectors, so the total effect of shocks is magnified as the shocks propagate through the production network.

While I mostly focus my robustness analysis on the unconstrained worst-case amplification, I also study the sensitivity to what I call static-neutral shocks. These are network inputs that can have an aggregate effect on output through dynamic propagation and the reallocation of activity across sectors, but have no permanent effect. The empirical application shows that the US production network is susceptible to dynamic sectoral reallocations of economic activity, between final-demand-intensive sectors and sectors more important as inputs in production, that are by construction not detectable in a static setting.

2. Motivating Example

To motivate my main framework, I discuss the primary application that I focus on in this paper, the dynamic production network model of Long and Plosser (1983). I also briefly outline a second class of applications, a model of information propagation following DeGroot (1974), that I develop in more detail in the companion paper Williams (2026).

2.1 *Production Networks*

In the Long and Plosser (1983) model, sectoral interconnections give rise to aggregate dynamics. The economy consists of N sectors, each producing a distinct perishable good that can be used either as an intermediate input in production or consumed directly. Each sector is operated by a representative firm that combines labor and intermediate inputs from other sectors to produce output. The production function for firm i in period $t+1$ is given by

$$Y_{i,t+1} = Z_{i,t+1} L_{i,t}^{1-\beta_i} \prod_{j=1}^{N} X_{ij,t}^{a_{ij}},$$

where $L_{i,t}$ is labor employed by firm i, $X_{ij,t}$ is the quantity of good j used by firm i as an input, and $Z_{i,t+1}$ is a stochastic productivity shock. Here $\sum_j a_{ij} \equiv \beta_i$ is the input share of

firm i, with $1-\beta_i$ being the labor share. Labor represents a "leakage" from the network, so input shares govern the speed of propagation and play a key role in the analysis.

As is well known, when consumers have logarithmic utility, the equilibrium dynamics have a closed-form solution.[12] The log of sectoral output evolves according to

$$\log Y_{i,t+1} = k_i + \sum_{j=1}^{N} a_{ij} \log Y_{j,t} + \log Z_{i,t+1},$$

where k_i is a constant and a_{ij} is the share of good j used by sector i in production.

Vectorizing this system across sectors, letting $x_t = \log Y_t - \log \bar{Y}$ denote log deviations from steady state, and using the corresponding Euler continuous-time embedding, we can write the dynamics as:

$$\dot{x} = -(\mathrm{I} - A)x + z \equiv -Lx + z, \tag{1}$$

where A is the matrix of input-output coefficients, and z collects the productivity shocks. Here $L = \mathrm{I} - A$ is a Laplacian operator that governs the flow of shocks through the production network. If there were no labor input so $\beta_i \equiv 1$, then constant returns to scale would make the matrix A row-stochastic with unit input shares. In this case, the operator L is a random-walk graph Laplacian, a key object in the analysis of dynamic processes on networks. But here I assume that each sector uses labor, so intermediate shares satisfy $\beta_i < 1$. Thus the adjacency A is sub-stochastic and $-L$ is a Hurwitz matrix, so the production network is dynamically stable. The Laplacian dynamics propagate sectoral shocks over time across the network, but their effects decay due to leakage into labor.

Much of the subsequent literature, as discussed in Carvalho and Tahbaz-Salehi (2019), has used a static version of this model to study the long-run cross-sectional diffusion of shocks. In the static setting, output is determined by the fixed-point equation

$$x = Ax + z \quad \Rightarrow \quad x = (\mathrm{I} - A)^{-1} z,$$

where $(\mathrm{I}-A)^{-1}$ is the so-called Leontief inverse. This matrix captures the full set of direct and indirect input relationships among sectors and admits the power series expansion

$$(\mathrm{I} - A)^{-1} = I + A + A^2 + A^3 + \dots.$$

The (i, j) entry measures the cumulative influence of sector j on sector i through all input chains of any length.

I incorporate dynamics both through output that evolves according to the differential equation above, and through dynamic shocks $z(t)$ that may evolve over time, possibly stochastically or with persistent autocorrelation. I develop an approach to analyze uncertainty in both the shocks and the network structure, providing a general treatment of uncertainty and shock transmission in networked economies.

The production network is a weighted, directed graph. Each node represents a sector, and a directed edge weight a_{ij} reflects the share of input j used by firm i. Because

[12] More detail on the derivation is provided in Appendix A.1.

these flows are inherently directional, the corresponding adjacency matrix A is generally asymmetric, although I develop some analytic results below in the special cases where networks are symmetric, or where all sectors have a common input share parameter $\beta_i = \beta < 1$.

2.2 *Information Propagation and Consensus*

Beyond the input-output model, my methods cover a broad class of network-based propagation and diffusion dynamics. One example is a version of the DeGroot (1974) model of learning in a social network.[13] Here, each node in the network represents an agent, and the state $x_i(t)$ is agent i's belief at time t about some underlying state of the world. Agents update their beliefs by listening to their neighbors, and also receive new information that shifts their beliefs. If agent i listens with weight a_{ij} to agent j, and receives a belief-shifting signal $u_i(t)$, then the dynamics become:

$$\dot{x}_i = \sum_j a_{ij}(x_j(t) - x_i(t)) + u_i(t) = -\sum_j L_{ij}x_j(t) + u_i(t),$$

which is a version of perturbed Laplacian dynamics as in (1). In Williams (2026), I apply the methods developed here to study disagreement dynamics on information networks.

3. Perturbed Network Dynamics

I now introduce methods from control systems to study perturbed network dynamics.

3.1 *Setup*

I work with a general network, represented by an $N \times N$ adjacency matrix A, and Laplacian $L = I - A$. I suppose that the output of interest is a linear combination of the state, represented by $y = Cx$, where C may select specific nodes or aggregate across the network. Then the general perturbed dynamic system is given by:

$$\begin{aligned} \dot{x} &= Mx + Bu, \\ y &= Cx, \end{aligned} \tag{2}$$

where $x \in \mathbb{R}^N$ is the state vector, u is an input or shock vector (which may differ in dimension from N), $M = -L = A - \mathrm{I}$, and B maps the input into the state space. This defines a continuous-time, linear, multi-input, multi-output (MIMO) control system.[14]

In the production model, the productivity shocks enter as exogenous stochastic inputs in this way, with (1) being a version of (2). In the consensus model, the input is exogenous news or information that affects agents directly. Beyond stochastic shocks, I describe below how $u(t)$ may represent uncertainty in the network or its dynamics. Mapping the network dynamics into a control system allows me to adapt control theory methods to evaluate the fragility and performance of networks under uncertainty.

[13] See also Jackson (2008) and Golub and Jackson (2010).

[14] See Skogestad and Postlethwaite (2005) for more background and details on such control systems. While the continuous time approach is slightly simpler, the results all have parallels in discrete time.

3.2 *Laplace Transform the Laplacian*

To analyze the dynamics and propagation of shocks, I use frequency domain tools from control theory. This allows for flexible treatment of how shocks and uncertainty propagate through a system. The Laplace transform is a classical tool that converts a time-domain system into the frequency domain. For a complex variable $s = \sigma + j\omega$ with $\sigma, \omega \in \mathbb{R}$ and $j = \sqrt{-1}$, the Laplace transform of a function $f : \mathbb{R}_+ \to \mathbb{R}$ is defined as

$$F(s) = \int_0^\infty e^{-st} f(t)\, dt.$$

Applying this to the linear control system $\dot{x} = Mx + Bu$, with initial condition $x(0) = 0$, we convert the dynamic system to an algebraic one:

$$\begin{aligned} sX(s) &= MX(s) + BU(s), \\ Y(s) &= CX(s), \end{aligned}$$

where $X(s)$, $U(s)$, and $Y(s)$ are the Laplace transforms of the state, input, and output vectors. Solving algebraically yields the transfer function:

$$Y(s) = C(sI - M)^{-1}BU(s) \equiv G(s)U(s),$$

which maps frequency-domain inputs $U(s)$ to outputs $Y(s)$. The transfer function $G(s)$ is the Laplace transform of the time-domain impulse response functions, and so provides a frequency-domain summary of the system's dynamic response to shocks.

3.3 *Static Limit: The Leontief Inverse*

One advantage of this framework is that it nests the familiar static analysis as the frequency zero limit: $s = 0$. Then the transfer function becomes

$$G(0) = C(-M)^{-1}B.$$

Now suppose $B = C = I$, which means that we have a full vector of inputs or shocks that can affect each state variable, and that the output of interest is the full state vector. Then, using the definition of M, $G(0) = (\mathrm{I} - A)^{-1}$ is exactly the Leontief inverse discussed above. This captures the long-run, steady-state response of the full cross-sectional output to a permanent unit shock to each sector.

The low frequency behavior is important, and I show below that some key properties of a class of models, which includes the production network model, are governed by their behavior at frequency zero. However, in dynamic settings, we are generally interested in the dynamic response of shocks, which may themselves have cross-sectional and temporal correlations. Thus to characterize the performance of a dynamic model in practical settings we need to analyze the response across the frequency spectrum. The transfer function $G(j\omega)$ captures the sensitivity of outputs to shocks at each frequency ω, allowing us to analyze how different types of shocks affect the system over time.

3.4 *MIMO Systems and Singular Values*

In the remainder of the paper I will follow the standard convention in control theory and use the same (lower-case) notation for both a variable in the time domain and its Laplace transform in the frequency domain.

In multi-input, multi-output (MIMO) systems, the transfer function $G(j\omega)$ is a matrix, and both input and output are vectors. To assess system performance, we study how $G(j\omega)$ transforms input vectors into output vectors. In a single-input, single-output system, the gain from input to output is just the magnitude of the transfer function, $|G(j\omega)|$. The appropriate multidimensional generalization is the largest singular value:

$$\overline{\sigma}(G(j\omega)) = \max_{u(\omega)\neq 0} \frac{\|G(j\omega)u(\omega)\|_2}{\|u(\omega)\|_2}.$$

This gives the maximum amplification at frequency ω, over all input directions $u(\omega)$.

Let $G^H = \left(\overline{G}\right)^T$ denote the Hermitian, or conjugate transpose, of a complex matrix G. Then the singular values of G are the square roots of the eigenvalues of $G^H G$:

$$\sigma_i(G) = \sqrt{\lambda_i(G^H G)}.$$

Recall as well that the matrix G is normal if $G^H G = GG^H$. Symmetric matrices, which govern the dynamics of undirected networks, are a special case of normal matrices, as are rotation matrices, which govern the dynamics of cyclical networks. For normal matrices, the singular values equal the absolute values of the eigenvalues, $\sigma_i(G) = |\lambda_i(G)|$. But for general asymmetric matrices, such as for general directed networks, there is no clear relation between the eigenvalues and singular values.

Parallel to eigenvectors, the left and right singular vectors are useful to diagnose input and output directions. The largest singular value of a matrix G satisfies:

$$\bar{\sigma}(G) = \max_{\|v\|_2=1} \|Gv\|_2 = \|G\|_2,$$

where the last equality defines the induced matrix 2-norm. A unit vector $\bar{v}$ achieving this maximum is a right singular vector, which solves $G^H G\bar{v} = \bar{\sigma}^2\bar{v}$. The corresponding left singular vector is $\bar{u} = G\bar{v}/\bar{\sigma}$, equivalently $GG^H\bar{u} = \bar{\sigma}^2\,\bar{u}$.

Most network analyses in economics focus on the eigenvalues and eigenvectors of the adjacency matrix A, but these need not capture dynamic amplification in the presence of asymmetry or non-normality. A normal matrix has orthogonal eigenvectors, which thus form a basis, and the eigenvalues capture how the system evolves. But when a matrix is not normal, its eigenvectors need not be orthogonal. The eigenvalues still measure how the system evolves along its eigenvectors, but in response to perturbations or inputs the system will rarely evolve in those directions. Any disturbance will activate distinct, interacting modes, and may produce amplification not captured by the eigenvalues. By contrast, singular values describe how the system transforms inputs into outputs, and hence here how shocks propagate. Singular vectors capture the interactions across modes, which may amplify or dampen the system's response to shocks. Thus singular values are key objects of the analysis, and eigenvalues are sufficient only when the network is normal.

3.5 *System Norms*

While the singular value at each frequency gives the maximum gain, to summarize the overall performance across frequencies, we compute norms of the transfer function.

The $\mathcal{H}_\infty$ norm measures the worst-case amplification from inputs to outputs across all directions and frequencies:

$$\|G(s)\|_\infty = \sup_\omega \overline{\sigma}(G(j\omega)) = \sup_\omega \max_{u(\omega)\neq 0} \frac{\|G(j\omega)u(\omega)\|_2}{\|u(\omega)\|_2} = \sup_\omega \|G(j\omega)\|_2 \tag{3}$$

This is the key object in robust control, and corresponds to the largest possible gain the system can produce, given any bounded input. This norm is especially relevant when the properties of the shocks or the network structure are uncertain. Rather than specifying the stochastic properties of the input $u(t)$, we treat it as an unknown but norm-bounded perturbation that represents an uncertain shock or modeling error. The $\mathcal{H}_\infty$ norm bounds the performance of the network in the presence of such uncertain inputs.

Alternatively, the $\mathcal{H}_2$ norm measures average performance across frequencies:

$$\|G(s)\|_2 = \sqrt{\frac{1}{2\pi}\int_{-\infty}^{\infty} \operatorname{tr}(G(j\omega)^H G(j\omega))\, d\omega} = \sqrt{\frac{1}{2\pi}\int_{-\infty}^{\infty} \sum_i \sigma_i^2(G(j\omega))\, d\omega}. \tag{4}$$

If $u(t)$ is a Gaussian white noise process and the state matrix M is Hurwitz, then $\|G(s)\|_2 = \sqrt{\mathbb{E}[y(t)^H y(t)]}$ is the steady-state root mean square magnitude of the output. While the $\mathcal{H}_\infty$ norm depends on the maximum singular value, the second expression above shows that all of the singular values, averaged across frequencies, contribute to the $\mathcal{H}_2$ norm.

Below I provide some general formulas for the $\mathcal{H}_2$ and $\mathcal{H}_\infty$ norms, as well as explicit examples in different settings. Before turning to these formulas, I discuss how the $\mathcal{H}_\infty$ norm provides a measure of robustness.

3.6 *Uncertainty and Robustness*

Dynamic networks are subject to a wide range of uncertainties. These may arise from changes or misspecification in the network itself, or in how outputs and inputs are measured or interact. By treating the input $u(t)$ as an uncertain input, the $\mathcal{H}_\infty$ norm provides a measure of the robustness of the system to misspecification.

A flexible approach to modeling uncertainty is to represent misspecification as a feedback distortion of the effective disturbance entering the model.[15] This means that the input $u(s)$ can consist both of specified shocks $u_0(s)$ and unknown modeling errors or uncertainty $\Delta(s)$ that may feed back on the output. Thus the actual system becomes:

$$y(s) = G(s)(u_0(s) + \Delta(s)y(s)) = G(s)u(s). \tag{5}$$

In Appendix A.2 I show that many forms of uncertainty can be mapped into, or bounded by, a representation like (5). This includes uncertainty about the network structure, such

[15] Hansen and Sargent (2008) have developed a related approach in economics.

as its parameters or dynamics, uncertainty about the structure or correlations of shocks, or uncertainty in output measurement due to aggregation, delay, or mismeasurement.

Imposing no structure on the uncertainty, I assume that the perturbation $\Delta(s)$ is stable and satisfies a uniform bound of $1/\gamma$ across all frequencies:

$$\|\Delta(s)\|_\infty \equiv \sup_{\omega\in\mathbb{R}} \bar{\sigma}(\Delta(j\omega)) < \frac{1}{\gamma}.$$

This captures the idea that the precise nature of the uncertainty is unknown, but its overall magnitude is limited. A fundamental result from robust control theory is the small gain theorem, which provides a sharp characterization of when a system remains stable in the face of such uncertainty. The theorem follows Zhou, Doyle, and Glover (1996), with proof outlined in Appendix A.3.

THEOREM 1. *Let $G(s)$ be the transfer function of a linear time-invariant system, and suppose that the uncertainty $\Delta(s) \in \mathcal{H}_\infty$ enters through the feedback interconnection* (5). *Suppose that $G(s)$ and $\Delta(s)$ are both stable transfer functions. Then the closed-loop system is internally stable for all $\Delta(s)$ satisfying $\|\Delta\|_\infty < 1/\gamma$ if and only if*

$$\|G\|_\infty \leq \gamma.$$

The transfer function $G(s)$ describes how shocks at different frequencies and across different nodes in the network are transmitted to outputs. If the worst-case amplification from input to output is large, then even modest misspecifications or input distortions can be destabilizing. By contrast, if $G(s)$ dampens shocks across all directions and frequencies, the system can tolerate a broader set of uncertainties without risk of instability. Thus I focus on the $\mathcal{H}_\infty$ norm of systems both as a way of gauging performance for arbitrary shocks and robustness to uncertainty.

4. CHARACTERIZATION OF PERFORMANCE AND ROBUSTNESS FOR NETWORK DYNAMICS

In this section I characterize both the average–case and worst–case amplification in network systems, using the $\mathcal{H}_2$ and $\mathcal{H}_\infty$ norms. For any matrix X, let X^H denote the Hermitian transpose when X is complex and the (regular) transpose when X is real.

4.1 *General Formulas for the System Norms*

4.1.1 *$\mathcal{H}_2$ Norm* I make the standard assumption that the input-output map as measured by the transfer function is stable, which ensures that the $\mathcal{H}_2$ norm is finite.[16] We can calculate the norm by solving a matrix Lyapunov equation, which effectively computes a steady-state covariance matrix, as shown in Appendix A.4.

[16]When the state matrix M is Hurwitz, as in production networks, then standard controllability and detectability conditions, as in Skogestad and Postlethwaite (2005), Chapter 4, suffice.

THEOREM 2. *Suppose M is Hurwitz, and let P be the unique solution of the continuous Lyapunov equation*

$$MP + PM^H + BB^H = 0.$$

Then

$$\|G\|_2^2 = \mathrm{tr}(CPC^H) = \mathrm{tr}(PC^HC). \tag{6}$$

If L, or equivalently M, is diagonalizable, we can write:

$$L = V\Lambda V^{-1}, \qquad M = -L = -V\Lambda V^{-1},$$

where $\Lambda = \mathrm{diag}(\lambda_i(L))$. Then define the modal projections

$$B_e = V^{-1}BB^HV^{-H}, \qquad S_e = V^HC^HCV.$$

Here B_e captures how shocks load onto modes, and S_e is how modes map into outputs. Then the Lyapunov equation in modal coordinates has solution $P = VYV^H$, where

$$Y_{ij} = \frac{B_{e,ij}}{\lambda_i + \overline{\lambda_j}}.$$

Thus we have the following result, adapted from Yadykin and Iskakov (2021), whose proof is in Appendix A.5.

THEOREM 3. *When L is diagonalizable, the $\mathcal{H}_2$ norm can be represented as:*

$$\|G\|_2^2 = \sum_{i,j} \frac{S_{e,ji}B_{e,ij}}{\lambda_i + \overline{\lambda_j}}. \tag{7}$$

This expression shows explicitly how the $\mathcal{H}_2$ norm depends on all of the modes and on the projections of B and C into the basis of the eigenvectors. Non-normality affects B_e and S_e, hence the weights placed on modal interactions. Slow modes, whose eigenvalues have small real parts, contribute disproportionately to the $\mathcal{H}_2$ norm.

4.1.2 *The $\mathcal{H}_\infty$ Norm* As above, the $\mathcal{H}_\infty$ norm measures the worst–case amplification of bounded–energy inputs, and can be written

$$\|G\|_\infty = \sup_{\omega\in\mathbb{R}} \bar{\sigma}\big(G(j\omega)\big) = \sup_{\omega\in\mathbb{R}} \bar{\sigma}\big(C(j\omega I - M)^{-1}B\big)\,.$$

The worst–case disturbance, both in direction and frequency, is the one whose image under the resolvent $(j\omega I - M)^{-1}$ is most strongly amplified by B and C. While the $\mathcal{H}_2$ norm reduces to a Lyapunov equation, here we do not have a closed form expression, but rather must take a supremum across frequencies.

If L is diagonalizable, denote the left and right eigenvalue-eigenvector pairs as $Lv_i = \lambda_i v_i$ and $w_i^HL = \lambda_i w_i^H$, where we normalize $w_i^Hv_j = \delta_{ij}$, the Kronecker delta. Then via

Sylvester's formula for analytic functions we can write the resolvent expansion[17]

$$(sI - M)^{-1} = (sI + L)^{-1} = \sum_i \frac{v_i w_i^H}{s + \lambda_i}.$$

Consequently we have the spectral expansion of the transfer function:

$$G(s) = C(sI - M)^{-1}B = \sum_i \frac{C v_i w_i^H B}{s + \lambda_i}.$$

Therefore we can write the $\mathcal{H}_\infty$ norm as:

$$\|G\|_\infty = \sup_{\omega \in \mathbb{R}} \bar{\sigma}\left(\sum_i \frac{C v_i w_i^H B}{j\omega + \lambda_i} \right). \tag{8}$$

This form makes explicit the contribution of each eigenvalue to the transfer function, with the numerator measuring how strongly that mode affects the input–output map.

4.2 *Positive Systems*

The average performance of the network, as measured by the $\mathcal{H}_2$ norm, typically depends on all frequencies. But for positive systems like production networks, the $\mathcal{H}_\infty$ robustness is governed by zero-frequency behavior. Precisely, for stable systems with nonnegative A, B, and C, the $\mathcal{H}_\infty$ norm always peaks at frequency zero. The result is adapted from Rantzer (2012), with proof in Appendix A.6.

THEOREM 4. *Let the adjacency matrix $A \geq 0$ have row sums $\sum_j A_{i,j} = \beta_i < 1$, and assume $B \geq 0$ and $C \geq 0$. Then*

$$\|G\|_\infty = \sup_{\omega \in \mathbb{R}} \|G(j\omega)\|_2 = \|G(0)\|_2 = \|CL^{-1}B\|_2 = \bar{\sigma}(CL^{-1}B).$$

With this result we can also diagnose the worst-case inputs and their output impacts. Let $\bar{v}$ and $\bar{u}$ be the right and left singular vectors corresponding to $\bar{\sigma}(CL^{-1}B)$. Then the worst-case input direction is $\bar{v}$:

$$\sup_\omega \max_{\{u : \|u\|_2 = 1\}} \|G(j\omega)u\|_2 = \|G(0)\bar{v}\|_2.$$

The corresponding most-sensitive output pattern is $\bar{u}$:

$$G(0)\bar{v} = \bar{\sigma}(CL^{-1}B)\,\bar{u}.$$

In Section 3.3 we showed that when $B = C = I$, then $G(0) = (I - A)^{-1}$. This is the Leontief inverse, the fundamental object of interest in static production network models. Theorem 4 shows that the worst-case amplification of disturbances in the dynamic

[17] See Lancaster and Tismenetsky (1985), Chapter 9.

system is governed precisely by the largest singular value of the Leontief inverse. The corresponding singular vectors identify the most destabilizing direction in input space, hence the most damaging pattern of sectoral shocks, and the most amplified direction in output space. I use this result below for different production network examples.

4.3 *Normal Matrices and Full State Analysis*

The system norms were given in modal form in (7) and (8) for general directed networks. But when the state dynamics are normal, as in undirected networks, these expressions simplify. When L is normal, we can write its diagonalization with a unitary matrix V:

$$L = V\Lambda V^H.$$

Hence we may choose an orthonormal eigenbasis:

$$v_i = Ve_i, \qquad w_i = v_i,$$

so that $w_i^H v_j = \delta_{ij}$.

I start with the $\mathcal{H}_2$ formula (7). With normal dynamics and $B = C = I$, the modal input and output weights become

$$B_{e,ij} = w_i^H BB^H w_j = w_i^H w_j = \delta_{ij}, \qquad S_{e,ji} = v_j^H C^H C v_i = v_j^H v_i = \delta_{ij},$$

so $B_e = S_e = I$ in the eigenbasis of L. Substituting into (7) gives

$$\|G\|_2^2 = \sum_{i,j} \frac{\delta_{ij}\,\delta_{ij}}{\lambda_i + \overline{\lambda_j}} = \sum_i \frac{1}{\lambda_i + \overline{\lambda_i}} = \frac{1}{2}\sum_i \frac{1}{\Re\lambda_i}. \tag{9}$$

In particular, when L is real and symmetric (so $\lambda_i \in \mathbb{R}_{++}$), this reduces to

$$\|G\|_2^2 = \frac{1}{2}\sum_{i=1}^N \frac{1}{\lambda_i} = \frac{1}{2}\,\mathrm{tr}(L^{-1})$$

For positive networks, from Theorem 4 the $\mathcal{H}_\infty$ norm with $B = C = I$ reduces to:

$$\|G\|_\infty = \bar{\sigma}(L^{-1}) = \max_i \frac{1}{|\lambda_i|} = \frac{1}{\min_i |\lambda_i|}. \tag{10}$$

When L is symmetric, the eigenvalues are strictly positive so the $\mathcal{H}_\infty$ norm is simply the inverse of the smallest eigenvalue.

Here both the $\mathcal{H}_2$ and $\mathcal{H}_\infty$ norms depend on the inverses of the eigenvalues of the Laplacian, or correspondingly the inverse of the distance between the eigenvalues of the adjacency matrix and one. For the $\mathcal{H}_2$ norm, all of the Laplacian eigenvalues matter, and the norm value is proportional to the sum of their inverses. For the $\mathcal{H}_\infty$ norm, only the smallest Laplacian eigenvalue, or largest adjacency eigenvalue, matters. As the system approaches instability, with smallest Laplacian eigenvalue approaching zero, both norms explode.

4.4 *Production Networks and Aggregate Output*

In many situations, we may care more about aggregate output than the whole cross-sectional output vector. Here I keep $B = I$, thus allowing for shocks to hit each sector, but then aggregate the sectoral outputs into a weighted total using an $N \times 1$ nonnegative weight vector $c \geq 0$. So $C = c^\top$ and the system output is $y_t = \sum_{i=1}^N c_i x_{i,t}$. In the theoretical examples below I set $c = 1_N$, while in the empirical application I set c equal to the sectoral GDP shares. I first show that the $\mathcal{H}_\infty$ norm has some interpretable implications for aggregate output in general production networks. Then I specialize to normal production networks, where the performance measures simplify.

4.4.1 *The $\mathcal{H}_\infty$ Norm in General* Since aggregate output is a scalar, the transfer function becomes a vector-valued function:

$$G(s) = c^\top (sI + L)^{-1}.$$

Then $G(0) = c^\top L^{-1}$ is a $1 \times N$ row vector with nonnegative elements, which we can write as $G(0) = [G_{0,j}]$ where:

$$G_{0,j} = \sum_{i=1}^N c_i \left(L^{-1}\right)_{i,j}. \tag{11}$$

Then the $\mathcal{H}_\infty$ norm is just the Euclidean norm of this vector:

$$\|G\|_\infty = \|G(0)\|_2 = \|c^\top L^{-1}\|_2 = \sqrt{\sum_{j=1}^N \left(\sum_{i=1}^N c_i \left(L^{-1}\right)_{i,j}\right)^2}.$$

Since $G(0)$ is a real vector, $\|G(0)\|_2$ is its only singular value, and the right singular vector is proportional to $L^{-\top} c$, the transpose of $G(0)$.

Recall that L^{-1} is the Leontief inverse of the production network. The inner sum in the expression above, $G_{0,j}$, is the weighted-total economy-wide output response to a unit shock applied at node j. In static production networks, Domar weights capture the response of output to sectoral productivity changes.[18] The multipliers $G_{0,j}$ play a similar role here, but now measure the aggregate output response to persistent sectoral shocks. The outer sum in the norm squares these multipliers and adds them up, providing a measure of the aggregate worst-case amplification of shocks across nodes. If shocks can hit multiple nodes in the network in correlated ways, the worst-case shock aligns with the vector of sectoral shocks with the largest weighted aggregate impact.

4.4.2 *Normal Dynamics* When the production network Laplacian L is normal, we can simplify the expressions for both performance measures when considering aggregate output. Using the same diagonalization as above, $L = V \Lambda V^H$, define the coordinates of the weight vector c in the eigenbasis of L by

$$\alpha = V^H c, \text{ with elements } \alpha_i = v_i^H c.$$

[18] See Carvalho and Tahbaz-Salehi (2019), for example.

Thus α_i measures the contribution of mode i to the c-weighted aggregate output. Then, using the $\mathcal{H}_2$ modal formula (7), we again have $B_e = I$ and $B_{e,ij} = \delta_{ij}$, but now the output projection term is:

$$S_{e,ji} = v_j^H C^H C v_i = v_j^H c c^\top v_i = (v_j^H c)(c^\top v_i) = \alpha_j \overline{\alpha}_i.$$

Then, since only the diagonal terms enter, we have:

$$\|G\|_2^2 = \sum_{i,j} \frac{\delta_{ij} |\alpha_i|^2}{\lambda_i + \overline{\lambda_j}} = \sum_i \frac{|\alpha_i|^2}{\lambda_i + \overline{\lambda_i}} = \frac{1}{2} \sum_i \frac{|\alpha_i|^2}{\Re \lambda_i}. \tag{12}$$

Further, when L is symmetric, by the spectral decomposition $L^{-1} = \sum_i \lambda_i^{-1} v_i v_i^\top$, hence

$$\|G\|_2^2 = \frac{1}{2} \sum_i \frac{|\alpha_i|^2}{\lambda_i} = \frac{1}{2} c^\top L^{-1} c.$$

The expression (12) is similar to (9) for the full output vector. But now the impact of each eigenvalue λ_i is weighted by $|\alpha_i|^2$, which measures how aligned mode i is with aggregate output. As before, slow-decaying modes with small $\Re \lambda_i$ generate large internal amplification. But now if $|\alpha_i|$ is large, then eigenvector v_i involves many firms responding in the same direction or in a way that has a large influence on aggregate output. So the impact of a mode on the volatility of aggregate output depends both on how it impacts sectoral volatility, and how that sectoral volatility feeds into aggregate volatility.

For the $\mathcal{H}_\infty$ norm, we can use the diagonalization to specialize:

$$G(0) = c^\top L^{-1} = c^\top V \Lambda^{-1} V^H = \alpha^H \Lambda^{-1} V^H.$$

Then taking the norm of this vector leads to the result:

$$\|G\|_\infty^2 = \alpha^H \operatorname{diag}\Big(\frac{1}{|\lambda_i|^2}\Big) \alpha = \sum_{i=1}^N \frac{|\alpha_i|^2}{|\lambda_i|^2}. \tag{13}$$

For aggregate output, the two measures of system performance are more similar than when focused on the full cross-sectional output vector. Here both depend on all of the system modes through the sums involving $|\alpha_i|^2$, the mode's contribution to aggregate output, and on a feature of the corresponding eigenvalue. For $\mathcal{H}_2$ the real part of the eigenvalue is what matters for overall volatility, while for $\mathcal{H}_\infty$ the magnitude of the eigenvalue is what matters for maximum amplification. When analyzing the full output cross-section with $C = I$ above, the worst-case disturbance is concentrated on the least-stable mode. But when aggregating from the cross-section, every mode matters, depending on how slowly it decays and how much it contributes to aggregate output, even in the worst case.

4.5 *Static-Neutral Shocks and Restricted Dynamic Amplification*

The robustness problems considered so far have been unrestricted, and we saw that for stable production networks with nonnegative input and output maps, the $\mathcal{H}_\infty$ norm

is attained at frequency zero. This applies both to cross-sectional output ($C = I$) and to aggregate output ($C = c^\top$). In each case, the unrestricted worst-case disturbance is governed by the corresponding static Leontief object $CL^{-1}B$.

In this section, I study a different problem. Rather than allowing all potential shocks, I restrict the shock or input space to those that have no static aggregate effect. The restriction fixes the aggregate steady state of the network, and instead focuses on its robustness to inputs that may propagate but have no permanent aggregate effect. Any aggregate response then comes from dynamic propagation and the reallocation of activity across sectors. In addition to providing additional diagnostics for network performance, this approach is useful for situations where we are more confident about the long-run properties of a model. A common practical approach is to analyze local fluctuations around a steady state, which naturally leads to a focus on higher-frequency robustness. Moreover, Onatski and Williams (2003) argued that monetary policymakers may be focused on smoothing business-cycle fluctuations, and thus interested in uncertainty over that frequency band.

For a permanent shock z, the long-run sectoral response is $L^{-1}z$, and the corresponding static aggregate effect is $c^\top L^{-1}z$. Then define $q \equiv L^{-\top}c$ as the vector of static aggregate exposures to primitive productivity shocks. I call a primitive shock vector z static-neutral if it has zero static aggregate effect:

$$q^\top z = c^\top L^{-1} z = 0.$$

Let

$$\mathcal{S} = \{z \in \mathbb{R}^N : q^\top z = 0\} \tag{14}$$

denote the subspace of static-neutral shocks. I now find a convenient representation for this space. Let $B_{\mathcal{S}} \in \mathbb{R}^{N\times(N-1)}$ be any orthonormal basis for the subspace $\mathcal{S}$:

$$q^\top B_{\mathcal{S}} = 0, \qquad B_{\mathcal{S}}^\top B_{\mathcal{S}} = \mathrm{I}_{N-1},$$

which is equivalently the null space of $q^\top$. The basis is not unique, but the performance norms do not depend on the basis.

Thus far, I have focused on unrestricted shocks hitting all sectors by setting $B = \mathrm{I}$, but now focus on static-neutral shocks by setting $B = B_{\mathcal{S}}$. The static-neutral transfer function can then be written:

$$G_{\mathcal{S}}(s) = c^\top (sI + L)^{-1} B_{\mathcal{S}}. \tag{15}$$

This is the ordinary aggregate output transfer function of the same production network, but with shocks restricted to the neutral subspace. Its $\mathcal{H}_\infty$ norm is:

$$\|G_{\mathcal{S}}\|_\infty = \sup_{\omega\in\mathbb{R}} \left\| c^\top (j\omega I + L)^{-1} B_{\mathcal{S}} \right\|_2.$$

Because $B_{\mathcal{S}}$ has orthonormal columns, this is exactly the largest gain over unit-norm shocks satisfying the constraint $q^\top z = 0$. By construction,

$$G_{\mathcal{S}}(0) = c^\top L^{-1} B_{\mathcal{S}} = q^\top B_{\mathcal{S}} = 0.$$

Thus every admissible shock in this problem is invisible to the aggregate-output calculation at frequency zero, and hence would not show up in a static analysis. Any nonzero aggregate response to such a shock must therefore be a dynamic propagation effect.

Since any nonzero vector orthogonal to a positive vector q must contain both positive and negative components, the input matrix $B_{\mathcal{S}}$ is no longer nonnegative, and hence the restricted transfer function in (15) does not satisfy the conditions of Theorem 4. The most-damaging static-neutral shocks thus generally occur at an interior frequency, as the next result makes formal. Its proof is given in Appendix A.7.

PROPOSITION 1. *Suppose $M = A - \mathrm{I}$ is Hurwitz. Let $q = L^{-\top}c$, and let $B_{\mathcal{S}}$ be any orthonormal basis for the space $\mathcal{S}$ in (14), with $G_{\mathcal{S}}(s)$ the corresponding transfer function (15). If $G_{\mathcal{S}}(s)$ is not identically zero, then its $\mathcal{H}_\infty$ norm is attained at a finite nonzero frequency:*

$$\|G_{\mathcal{S}}\|_\infty = \|G_{\mathcal{S}}(j\omega^*)\|_2 \qquad \textit{for some } |\omega^*| > 0.$$

The corresponding $\mathcal{H}_2$ norm has the usual Lyapunov representation, as in Theorem 2. If u_t is standard white noise in the static-neutral coordinates, then the input covariance in primitive shock space is $B_{\mathcal{S}}B_{\mathcal{S}}^\top = \Sigma_{\mathcal{S}}$. Let $P_{\mathcal{S}}$ solve

$$LP_{\mathcal{S}} + P_{\mathcal{S}}L^\top = \Sigma_{\mathcal{S}}.$$

Then

$$\|G_{\mathcal{S}}\|_2^2 = c^\top P_{\mathcal{S}} c.$$

Thus $\Sigma_{\mathcal{S}}$ removes the static aggregate shock direction from the input covariance, so the $\mathcal{H}_2$ norm here measures the aggregate volatility generated by static-neutral shocks.

The static-neutral subspace $\mathcal{S}$ allows the worst-case shock to offset arbitrary sectors against one another. In empirical applications it may be more natural to impose neutrality within economically meaningful blocks. For example, fine industries can be grouped into coarser production sectors, and we may wish to focus on shocks that reallocate activity across industries within a sector. A straightforward extension of the approach here can build in additional restrictions such as block neutrality.

5. ILLUSTRATIVE EXAMPLES

In this section I apply the analysis above to several illustrative network structures. I show how the average-case volatility ($\mathcal{H}_2$) and worst-case robustness ($\mathcal{H}_\infty$) depend on the network topology. I start with some examples with normal dynamics, which highlight the role of labor as a dampening factor which stabilizes the system. Then I illustrate some implications of non-normality, which is the empirically relevant case. I consider both cross-sectional output where $C = I$ and aggregate output where $C = 1_N^\top$.

5.1 *Examples with Normal Dynamics*

With normal dynamics we can calculate the performance norms via components of the Laplacian spectrum. The following examples use spectral characterizations of some classical graphs in the literature. These allow me to illustrate analytically how the performance measures depend on the network properties, and to isolate how network connections and the speed of adjustment can combine to create bottlenecks and amplification. Appendix B provides detailed calculations as well as additional examples.

5.1.1 *The Role of Labor in Production Networks* The simplest normal production networks are symmetric, with a homogeneous intermediate input share β. We can represent these with a baseline row-stochastic matrix A_0, where the production network is $A = \beta A_0$. Since A_0 has a unit eigenvalue, the largest eigenvalue of A is β. Therefore, in all cases regardless of the details of the network structure, the $\mathcal{H}_\infty$ norm in (10) is simply

$$\|G\|_\infty = \frac{1}{1-\beta}.$$

Further, the constant vector $v_1 = \frac{1}{\sqrt{N}} 1_N$ is the eigenvector associated with the Laplacian eigenvalue $1-\beta$. Since L is normal, its other eigenvectors are orthogonal to v_1. Hence we have $\alpha_1 = v_1^\top 1_N = \sqrt{N}$ while $\alpha_i = v_i^\top 1_N = 0$ for $i = 2, \ldots, N$. For aggregate output, (12) and (13) reduce to:

$$\|G\|_2^2 = \frac{N}{2(1-\beta)}, \qquad \|G\|_\infty = \frac{\sqrt{N}}{1-\beta}.$$

Thus these performance metrics only depend on the size of the network and the intermediate input share β, but not on any other aspect of the network structure.

For production networks, labor (or other non-networked inputs) gives a type of leakage from the network that dampens the impact of shocks. For symmetric networks with identical labor shares, this dampening is uniform. Thus for $\mathcal{H}_\infty$, the worst-case amplification occurs with a uniform shock to all sectors, giving simple expressions for the cross-sectional and aggregate amplification. For the $\mathcal{H}_2$ norm, all modes of the network matter and affect cross-sectional output volatility. But for aggregate output, the idiosyncratic effects of the individual sectors largely cancel. The network propagates only the common component of shocks, which is uniformly damped by labor. Thus a sparse production network can generate substantial sectoral dispersion and slow reallocation dynamics, while still leaving aggregate volatility comparatively muted.

Non-normal production networks arise generically, as purchasing and supplying relationships are rarely symmetric. But even when connections are symmetric, heterogeneity in input shares typically renders the resulting dynamics non-normal. In this section, I use a convenient specification of input share heterogeneity which preserves normality. Starting with a common reference value β, I define a sectoral perturbation vector $\Gamma = \mathrm{diag}(\beta_1 - \beta, \ldots, \beta_N - \beta)$, and set the adjacency matrix to:

$$A = \beta A_0 + \Gamma.$$

This introduces heterogeneous input shares by altering the diagonal of the adjacency, so sectors with lower input shares use less of their own goods as inputs. This specification preserves normality, since if A_0 is symmetric then A is as well. The Laplacian is then:

$$L = I - A = I - \beta A_0 - \Gamma = D - \beta A_0, \text{ where:}$$
$$D = \operatorname{diag}(d_1, \ldots, d_N), \;\; d_i = 1 - \beta_i + \beta.$$

I show how input share heterogeneity affects network dynamics by changing the effective weights of different modes, and hence the local speed of adjustment.

5.1.2 *Complete Network* I start with the symmetric complete network, which illustrates the extreme of connectedness and redundancy with each node connected to every other node. This represents thick interactions, with multiple suppliers and buyers in the production context, and diffuse propagation of information in the learning context. Here the baseline adjacency matrix is

$$A_0 = \frac{1}{N} 1_N 1_N^\top.$$

I focus here on the cross-section $C = \mathrm{I}$, while Appendix B.1 discusses aggregate output. With homogeneous input shares, the Laplacian $L = I - \beta A_0$ has eigenvalues $\lambda_1 = 1 - \beta$, $\lambda_2 = \cdots = \lambda_N = 1$, as discussed in Appendix B.1. From above, we know that the $\mathcal{H}_\infty$ norm is $1/(1-\beta)$ and the worst-case input is a uniform perturbation across sectors at frequency zero. For average performance we use (9):

$$\|G\|_2^2 = \frac{1}{2} \sum_{i=1}^{N} \frac{1}{\lambda_i} = \frac{1}{2} \left(\frac{1}{1-\beta} + N - 1 \right).$$

Thus cross-sectional volatility depends on the common component $1/(1-\beta)$ as in the worst-case amplification, but also on the idiosyncratic components which are orthogonal to it. As the size of the network grows, these idiosyncratic components contribute proportionally to overall volatility.

Introducing heterogeneous labor shares as above, recall that $d_i = 1 - \beta_i + \beta$, and define the following:

$$s_1 = \sum_{i=1}^{N} \frac{1}{d_i}, \qquad s_2 = \sum_{i=1}^{N} \frac{1}{d_i^2}, \qquad \eta = 1 - \frac{\beta}{N} s_1.$$

A small intermediate share β_i means a large d_i and more rapid adjustment in that sector. In Appendix B.1, I show that we can write the cross-sectional $\mathcal{H}_2$ norm as:

$$\|G\|_2^2 = \frac{1}{2} \operatorname{tr}(L^{-1}) = \frac{1}{2} \left(s_1 + \frac{\beta}{\eta N} s_2 \right).$$

The first term in s_1 aggregates sector-level persistence induced by heterogeneous labor shares, capturing how long shocks survive locally before being dissipated. The second term captures the network feedbacks. β/N reflects the strength of uniform mixing in

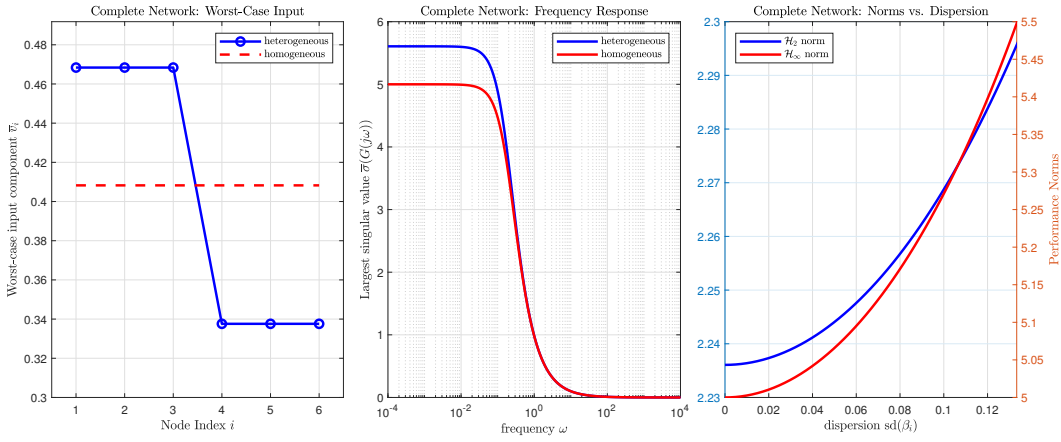


FIGURE 1. Left panel: Worst-case input vector $\overline{v}$ for a 6 node complete production network with heterogeneous and homogeneous labor shares. Center panel: largest singular values under homogeneity, with $\beta = 0.8$, and heterogeneity, where 3 sectors have $\beta_i = 0.933$ and 3 have $\beta_i = 0.667$. Right panel: $\mathcal{H}_2$ and $\mathcal{H}_\infty$ performance norms for complete networks with the two–type heterogeneity with varying dispersion.

the complete network, while η measures the distance to the stability boundary of the aggregate mode. The s_2 term puts extra weight on the most persistent sectors. A sector with high persistence accumulates its own volatility and disproportionately influences aggregate dynamics when sectors interact.

The eigenvalues of L are no longer directly related to those of L_0. I show in Appendix B.1 that the eigenvalues are given by the roots of

$$1 - \frac{\beta}{N}\sum_{i=1}^{N}\frac{1}{d_i - \lambda} = 0. \tag{16}$$

This equation determines the effective rate at which a common disturbance is dissipated once heterogeneity in labor or intermediate shares is taken into account. The smallest eigenvalue $\underline{\lambda} = \min_i \lambda_i$ is the smallest root of (16), and the components of its corresponding eigenvector can be written $\overline{v}_i = \frac{v_0}{d_i - \underline{\lambda}}$ for some constant $v_0 \neq 0$.

Thus the $\mathcal{H}_\infty$ norm captures how heterogeneous sectoral adjustment rates interact with uniform linkages to slow down the dissipation of shocks. When some sectors have high intermediate shares (hence low d_i), the aggregate mode becomes more persistent, increasing worst-case amplification even though the underlying network remains symmetric. Sectors with high intermediate shares receive disproportionately large weight in the worst-case disturbance. The most damaging disturbance concentrates on those sectors where shocks dissipate slowly. The network then redistributes these persistent local disturbances evenly across the economy through the complete mixing structure.

These results are illustrated in Figure 1, which considers a six-node complete production network with homogeneity and heterogeneity of labor shares. In the left and center panels the homogeneous case has $\beta = 0.8$ while under heterogeneity the first

three sectors have $\beta_i = 0.933$ and the last three have $\beta_i = 0.667$, and hence the same mean. The left panel shows the elements of the worst-case input vector $\overline{v}$, while the center panel shows the largest singular value $\overline{\sigma}(G(j\omega))$. In the homogeneous case, the worst-case input is a constant vector and the $\mathcal{H}_\infty$ norm is $1/(1-\beta) = 5$. Under heterogeneity, the worst-case input is constant across sectors with same labor share, but concentrates mass in the bottleneck sectors with larger β_i.[19] The center panel shows that heterogeneity increases the maximum amplification of shocks, as the peak of the singular values increases.[20] The right panel shows this result more broadly, plotting the $\mathcal{H}_2$ and $\mathcal{H}_\infty$ norms for this two-type form of heterogeneity, where we fix the mean input share at 0.8 and vary the dispersion. More sectoral dispersion increases overall volatility and especially worst-case amplification.

5.1.3 *Path Graph* While all nodes are symmetric with dense interactions in the complete network, in a path graph all nodes only interact with their neighbors in a longer chain. This is an example of thin markets and propagation with location effects, as the total impact of a bottleneck depends on where it lies along the chain.

Let A_0 be the symmetric row-stochastic path graph on $\{1,\dots,N\}$, where $A_{0,ij} = \frac{1}{2}$ when $i = j = 1$, $i = j = N$, or $|i-j| = 1$, and is zero otherwise. As I show in Appendix B.2, with homogeneous labor shares the eigenvalues of the Laplacian are:

$$\lambda_i = 1 - \beta \cos\left(\frac{(i-1)\pi}{N}\right), \qquad i = 1,\dots,N.$$

The path network has very low connectivity, as measured by the second smallest Laplacian eigenvalue. For large N, the connectivity of the baseline path network scales like N^{-2}, in comparison to the constant connectivity of the complete network.

As before, the $\mathcal{H}_\infty$ norm collapses to $1/(1-\beta)$, while the $\mathcal{H}_2$ aggregates the spectrum:

$$\|G\|_2^2 = \frac{1}{2}\sum_{i=1}^{N}\left(1 - \beta\cos\left(\frac{(i-1)\pi}{N}\right)\right)^{-1}.$$

Even though worst-case amplification is pinned down by the "leakage" $(1-\beta)$ from labor, the path creates many slow spatial modes that contribute disproportionately to $\mathcal{H}_2$. Local shocks propagate gradually through neighboring links, increasing the overall cross-sectional volatility even though the worst case is pinned down by the labor share.

Sectors with smaller than average labor shares, which adjust more slowly, become bottlenecks that contribute more to volatility and thus receive larger weight in the worst-case input. I show in Appendix B.2 that this holds for both cross-sectional and aggregate output. Because interactions are local, volatility depends on the location of the bottlenecks, not only on how many there are. This is illustrated in Figure 2, which shows the components of the worst-case input $\overline{v}$ for two networks that differ only in the location of the bottleneck sector with the smallest labor share, either in the middle or at one end

[19] Since the nodes are symmetric, the labeling and ordering are arbitrary. The apparent local concentration reflects the high β_i sectors being ordered first.

[20] Numerically, the $\mathcal{H}_\infty$ norm increases from 5 to 5.61 and the $\mathcal{H}_2$ norm increases from 2.24 to 2.31

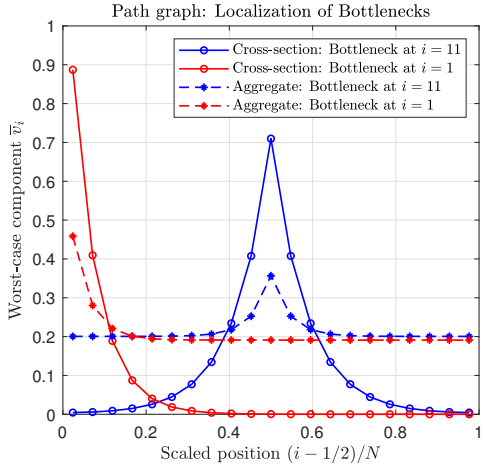


FIGURE 2. Worst-case input vector $\overline{v}$ for two production networks differing only in the location of the sector with the smallest labor share. Solid lines are for cross-sectional output, while dashed lines are for aggregate output.

of the chain.[21] The solid lines in the figure show the cross-sectional analysis here, while the dashed lines are for aggregate output. The results are similar, but because it weights the common component of output, the worst-case shocks are much less concentrated for aggregate output.

No matter where it is located, the bottleneck sector receives the highest weight in the worst-case input. Nearby sectors, which are homogeneous and are only distinguished by proximity to the bottleneck, also receive weight that diminishes in distance from the bottleneck sector. When the bottleneck is at the end, shocks can only move up the chain. When the bottleneck sector is in the center of the chain, shocks propagate both up and down the line, which allows the impact of a shock to be spread across more dissipative sectors, reducing both overall volatility and worst-case amplification.[22]

5.2 *Non-Normal Dynamics*

The previous examples illustrated features of network dynamics analytically, relying on the structure provided by normal dynamics. However, once we allow for direction, asymmetry, and heterogeneity, normality is clearly an exceptional special case. When the dynamics become non-normal, eigenvectors need not be orthogonal and modes interact, creating shock patterns and amplification different from what the eigenvalues alone would predict.

In the normal case I drew on known results for the spectra of classes of graphs, but there are many fewer analytic characterizations of non-normal singular value decompositions. In this section, I focus on versions of directed cycles with heterogeneous input shares, where dynamics are non-normal but can be explicitly characterized.

[21] Specifically, the figure uses $N = 21$ sectors, where 20 of them have $\beta_i = 0.6$, but one has $\beta_i = 0.95$.

[22] Numerically for cross-sectional output, with the bottleneck at the end, the $\mathcal{H}_\infty$ norm is approximately 4.73 and $\mathcal{H}_2$ is 3.86. With the bottleneck in the middle, the $\mathcal{H}_\infty$ norm is approximately 3.27 and $\mathcal{H}_2$ is 3.77.

5.2.1 *A Small Non-Normal Example* Economically, a directed cycle represents thin input and output markets, where a sector buys intermediates from a single upstream supplier and sells to a single downstream customer. I start with the simplest such case.

Consider a simple 2-sector production network where neither sector uses its own good as an input, and they have different intermediate shares, β_1 and β_2, each strictly between zero and one. Then the adjacency matrix A and Laplacian L are:

$$A = \begin{bmatrix} 0 & \beta_1 \\ \beta_2 & 0 \end{bmatrix}, \qquad L = \begin{bmatrix} 1 & -\beta_1 \\ -\beta_2 & 1 \end{bmatrix}.$$

Previously, I introduced share heterogeneity by varying how much of its own input each sector used, while here I directly vary the weight on other sectors. When $\beta_1 < \beta_2$, sector 1 is relatively less dependent on sector 2's good as an input, with sector 2 relatively more dependent on sector 1. The eigenvalues of L are $1 \pm \sqrt{\beta_1\beta_2}$ and hence only depend on the product of the shares. But as long as $\beta_1 \neq \beta_2$, L is non-normal.

The results of this section are illustrated in Figure 3. In Appendix B.3, I provide the analytic results underlying the figure, while here I interpret them. The left panel shows the $\mathcal{H}_\infty$ and $\mathcal{H}_2$ norms for this 2-sector directed production network, focusing on cross-sectional output $C = I$. The plot fixes the product of the input shares at $\beta_1\beta_2 = 0.25$, and hence fixes the Laplacian eigenvalues, and shows the norms for varying β_1. The center panel plots the elements of the corresponding worst-case input vector $\overline{v}$ as β_1 varies. The figure clearly shows that increasing sectoral heterogeneity increases both worst-case amplification and output volatility. The worst-case input vector loads more heavily on the sector with the smaller input share coefficient. The right panel shows the frequency response for aggregate output in the baseline network, which peaks at frequency zero, as well as for static-neutral shocks, which peaks at an interior frequency.

In a two-sector production chain, β_1 and β_2 measure how strongly each sector relies on the other. The eigenvalues of L reflect the average strength of the feedback loop between sectors through the product $\beta_1\beta_2$. By contrast, the singular vectors emphasize directionality. If one link is strong and the other is weak, then disturbances can be transformed as they circulate. The operator $LL^\top$ aggregates these "out-and-back" effects, and its eigenvectors identify disturbance patterns that are hard for the network to dissipate.

When the sectors have different input intensities, output volatility increases and the network becomes more fragile. When $\beta_2 > \beta_1$, sector 2 relies more heavily on sector 1 than vice versa. Sector 1 is therefore more upstream, as shocks to sector 1 propagate strongly to sector 2, while sector 2 shocks feed only weakly to sector 1. This directional imbalance shifts the worst-case amplification toward disturbances concentrated in sector 1, even when the overall loop strength $\beta_1\beta_2$, and hence the spectrum, is unchanged.

As shown in Appendix B.3, the static-neutral shocks have a direct interpretation in this example, especially when $c = [1, 1]^\top$. The static-neutral transfer function is maximized at the interior frequency determined by the overall loop strength

$$\omega^* = \sqrt{1 - \beta_1\beta_2}.$$

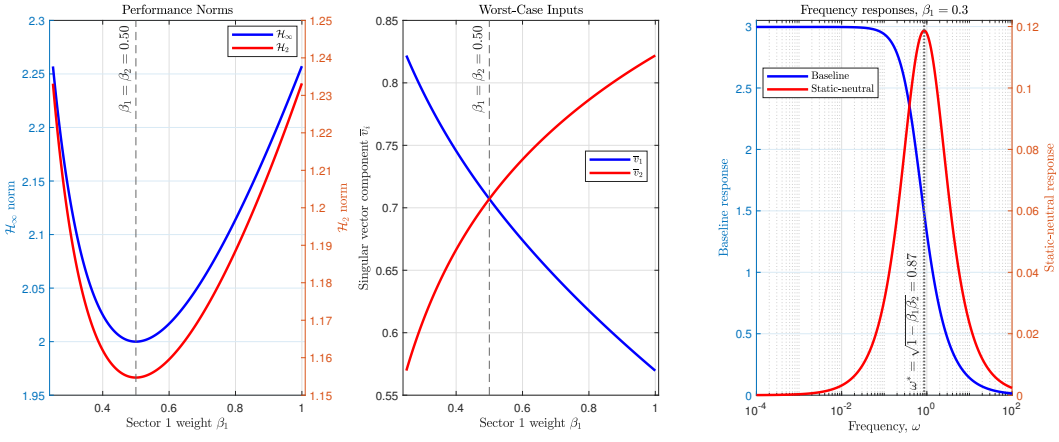


FIGURE 3. The left panel plots the $\mathcal{H}_\infty$ (left axis) and $\mathcal{H}_2$ (right axis) norms for a 2-sector directed production network. The sectoral input shares are β_1 and β_2, with fixed product $\beta_1\beta_2 = 0.25$, and the panel shows the norms for varying β_1. The center panel shows the corresponding worst-case input vector $\overline{v}$ as β_1 varies. The right panel shows, for $\beta_1 = 0.3$, the frequency responses for the baseline case (left axis) and static-neutral shocks (right axis).

The aggregate exposure vector q and static-neutral basis $B_{\mathcal{S}}$ are

$$q \propto \begin{pmatrix} 1+\beta_2 \\ 1+\beta_1 \end{pmatrix}, \qquad B_{\mathcal{S}} \propto \begin{pmatrix} 1+\beta_1 \\ -(1+\beta_2) \end{pmatrix}.$$

The vector $B_{\mathcal{S}}$ gives the direction of the static-neutral shock, which raises one sector and lowers the other in exactly the proportions that cancel the long-run aggregate effect. The corresponding worst-case disturbance is an oscillatory input at the frequency ω^*:

$$u(t) = B_{\mathcal{S}} \cos(\omega^* t).$$

At one phase of the cycle, the shock raises sector 1 and lowers sector 2, while half a cycle later the signs reverse. As long as $\beta_1 \neq \beta_2$ these sectoral composition shifts give rise to aggregate fluctuations.

This two-node example illustrates several features of non-normality in directed production networks. First, there is a clear divergence between the eigenvalues and the singular values, with the latter governing the response of the network to exogenous shocks. Holding fixed the product of the input shares fixes the eigenvalues, and hence common measures of the speed of convergence. But fixing the product while increasing the asymmetry between the two sectors increases both volatility and worst-case amplification of shocks. With this asymmetry, the worst-case inputs and most-amplified outputs differ when the network is directed. In this example, the difference is stark because an input which loads more heavily on one sector has the most impact on the output of the other. Systemic vulnerability reflects not only how strongly sectors are linked in aggregate, but how unevenly and directionally those linkages are organized, where the bottlenecks sit, and whether dependence is balanced across stages.

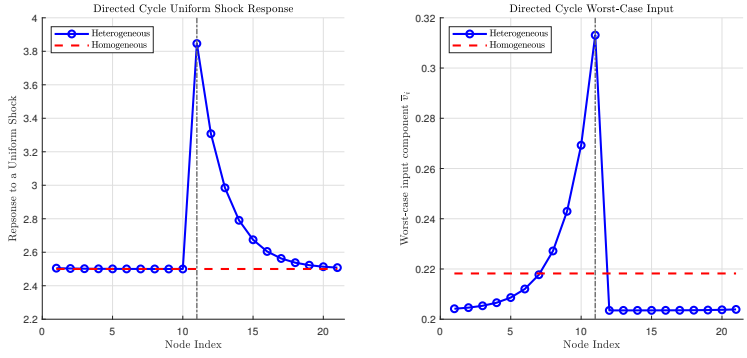


FIGURE 4. The left panel plots the sectoral steady-state response to a uniform shock and the right panel plots the worst-case input $\overline{v}$ for a 21-node directed cycle production network with aggregate output, where 20 sectors have $\beta = 0.6$ and one (node 11) has $\beta_{11} = 0.95$. The homogeneous case is shown for comparison.

5.2.2 *Directed Cycle Production Networks* The two-sector example is the smallest directed cycle and shows how asymmetry leads to a divergence between eigenvalues and singular values. I now embed the same mechanism in a larger directed cycle network with meaningful upstream and downstream locations. Here a localized bottleneck affects nearby sectors differently depending on their position in the cycle.

The general directed cycle is built on a row-stochastic adjacency matrix A_0 that shifts mass one step forward around the circle: $A_{0,i,i-1} = 1$ for $i = 2, \ldots, N$, $A_{0,1N} = 1$ and $A_{0,ij} = 0$ otherwise. This is an asymmetric but normal matrix, and as I discuss in Appendix B.4, with homogeneous labor shares it leads to a normal, directed production network. But it is no longer normal with heterogeneous labor shares.

In Appendix B.4, I consider cross-sectional output, and show that singular values of the non-normal production network differ from their eigenvalue counterparts. Since upstream and downstream effects are now distinct, the worst-case input vector is asymmetric. The worst-case input weights decay more rapidly downstream of a bottleneck than they do upstream.

Here I focus on aggregate output, where even under heterogeneity the sectoral multipliers $G_{0,j}$ from (11), giving the aggregate response to a persistent unit shock in sector j, have an explicit expression. Since aggregate output is a scalar, the worst-case input vector is then proportional to this multiplier vector. The multiplier vector satisfies $L^\top G(0)^\top = 1_N$, which here gives a recursion:

$$G_{0,i} = \frac{\beta}{d_i} G_{0,i+1} + \frac{1}{d_i}.$$

This recursion illustrates the directional propagation mechanism, as a low labor share sector (small d_i) amplifies multipliers upstream around the cycle until the effect wraps around. An explicit expression for $G_{0,i}$, from following a full lap around the cycle, is in the appendix. When one sector has a low labor share, shocks upstream of that bottleneck receive large aggregate multipliers.

These effects are illustrated in Figure 4 for a network with $N = 21$ nodes where node 11 has $\beta_{11} = 0.95$ and all other 20 sectors have $\beta = 0.6$. To illustrate the upstream and downstream effects of shocks, the left panel plots the sectoral steady-state response to a uniform shock, which is given by $L^{-1}1_N$. The asymmetries from the directed cycle are pronounced, as the responses are highest on the bottleneck sector and those immediately downstream from it, which are in the downstream "wake" of the amplification. This then affects how the multipliers and hence worst-case inputs are determined. The worst-case inputs are largest on the bottleneck sector and those immediately upstream, since upstream shocks feed most directly into the bottleneck and therefore affect aggregate output the most.

6. Fragility and Volatility in the US Production Network

I now apply my analysis to the US production network, showing how sectoral shocks and uncertainty are propagated to cross-sectional and aggregate output. As described in the appendix, the U.S. Bureau of Economic Analysis (2026) provides repeated cross-sections of detailed annual input-output tables roughly every five years, with the latest from 2017 for a 398-industry square network.[23] They also provide a consistent panel of 71 summary groups at the sectoral level, with annual data from 1997 to 2023. I first analyze how the level of aggregation in the network affects the network performance and fragility. While much of the networks literature has focused on how disaggregate "granular" shocks can generate aggregate fluctuations, I find that most of the volatility and robustness measures are largely governed by shocks at an intermediate, sectoral level. Then I analyze how changes in the production network over time have affected its volatility and fragility. I find that at a broad sectoral level the economy appears to have become less fragile over time. But at a finer disaggregation, fragility has increased and become more localized.

In Appendix C, I discuss the data sources and construction, and also provide additional related empirical results. As discussed in Appendix C.2, to focus on implications for aggregate output, I define the weight ν_i for sector i as the ratio of the sector's value-added to aggregate GDP. For the model's aggregate output I set $c = \nu$, while for cross-sectional output I set $C = \operatorname{diag}(\sqrt{\nu})$.[24] In the exercises below, I report the input energy share of sector i, which for the worst-case unit-norm vector at date t, $\bar{v}_t$, is simply $\bar{v}_{it}^2$. The effective number of sectors, $1/\sum_i \bar{v}_{it}^4$, is the number of equally-weighted sectors that would generate the same concentration. I use a similar effective concentration measure for other variables. While I have concentrated on the input share $\beta_i = \sum_j A_{ij}$, another indicator of sectoral importance is supplier strength, defined as $s_j = \sum_i A_{ij}$. This measures how intensively the output of sector j is used as an input across all producers.

[23] The BEA detailed data contains 402 industry groups, but only 398 codes appear both as industry columns and commodity input rows.

[24] As I discuss in the Appendix C.2, if ℓ_i is the sector's Domar weight, the ratio of sales or gross output to GDP, then $\nu_i = (1 - \beta_i)\ell_i$.

TABLE 1. Worst-case input sources for aggregate output in the 398-sector network

Rank	Sector	Energy	ν_i	β_i	s_i	Own	Direct	Total
1	Other real estate	0.192	0.026	0.590	6.986	0.012	0.014	0.036
2	Owner-occupied housing	0.136	0.068	0.137	0.000	0.025	0.000	0.025
3	Management of companies and enterprises	0.057	0.018	0.353	7.750	0.004	0.004	0.011
4	Monetary authorities & depository credit	0.053	0.022	0.331	2.622	0.005	0.002	0.010
5	State and local government (education)	0.043	0.038	0.195	0.000	0.008	0.000	0.008

6.1 *Fragility and Aggregation in the US Production Network*

The detailed 398-sector network displays quite a bit of heterogeneity in connectivity and weighting. The mean intermediate share β_i is 0.516 with a standard deviation of 0.176. As shown in the examples above, variation in intermediate shares affects the speed of adjustment to shocks and can lead to local bottlenecks. As I discuss in the appendix, changes in the data sources complicate temporal comparisons with the detailed network data, so I focus more on the sectoral input-output data below. But the 2017 detailed network can still provide insight on sources of fragility and volatility at a point in time.

Table 1 summarizes the five largest components in the worst-case input vector for aggregate output, along with some characteristics of the sector. The sectors with the largest GDP shares are not necessarily the most dangerous shock sources, although they are correlated. As shown in Appendix C.3, the worst-case energy is strongly correlated with GDP share ν_i, positively correlated with supplier strength s_i, and has a weak negative correlation with intermediate share β_i. The last three columns show the impact of the worst-case input $\bar{v}_i$ on aggregate output: its own immediate effect, $\nu_i \bar{v}_i$, the direct effect through the network, $(\nu^\top A)_i \bar{v}_i$, and the total steady-state effect, $(\nu^\top L^{-1})_i \bar{v}_i$.

The table illustrates how the different sectoral factors combine to determine how influential a sector is in aggregate fragility. Housing and state and local government education are final goods sectors ($s_i = 0$) with relatively low intermediate shares, and so play a less crucial role in transmitting shocks through the production network. But they are large sectors, 6.8% and 3.8% of GDP, and so have a large direct impact on aggregate output. The total effect of shocks to these sectors is the own impact. By contrast, other real estate and management of companies have high supplier strength, and so play a crucial role downstream as inputs in other sectors. In addition, real estate also has a large intermediate share, so it is crucially connected on both its input and customer chains. The total effects of shocks to these sectors are much larger than the own immediate effect. Altogether, a negative worst-case input looks like a real estate and financial recession, where losses in housing and other real estate combine with financial market and insurance (not shown, but in the top-ten sectors) disruptions to drive losses in management and the service sector.

Next I study how much volatility and amplification in the detailed network is lost by focusing on coarser levels of aggregation, where shocks and uncertainty are common to broader industry groups. For this I start with different levels of aggregation provided by

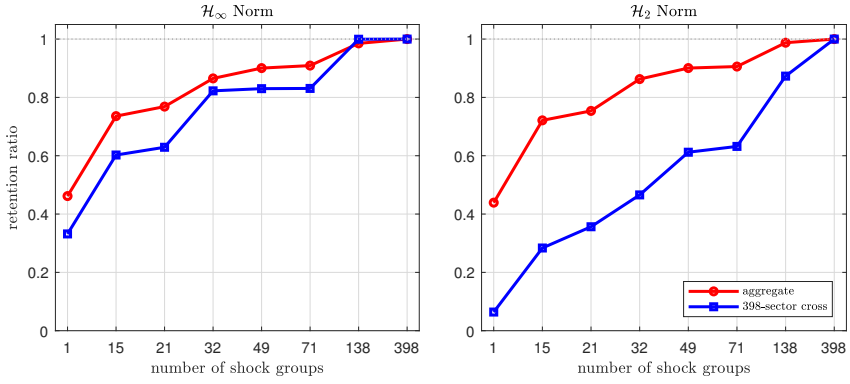


FIGURE 5. Retention of fragility ($\mathcal{H}_\infty$) and volatility ($\mathcal{H}_2$) for aggregate and cross-sectional output at different levels of aggregation, shown categorically with even spacing. The detailed 398-sector network is held fixed, while the inputs are restricted to coarser aggregations.

the BEA with 398, 138, 71, 21, and 15 industries or sectors. In addition, as detailed in Appendix C.3, I construct two levels with 49 and 32 sectors that aggregate some of the goods sectors from the 71-sector baseline, but keep the service sectors more disaggregated.

As I discuss in more detail in Appendix C.3, for this exercise I fix the detailed 398-sector network, but restrict the shock or uncertainty inputs to be common across the coarser aggregated groups. Figure 5 summarizes the results of this decomposition, showing how much the measures of aggregate and cross-sectional fragility and volatility are preserved at different levels of aggregation. Some sources of volatility and amplification are clearly lost in aggregation. The cross-sectional $\mathcal{H}_2$ decays sharply with aggregation, as the volatility of the full detailed output vector is sensitive to restricting directions of variation. But for the other measures relatively little is lost by aggregating from 398 to 71 or even 49 sectors. This aggregation preserves roughly 90% of the $\mathcal{H}_2$ and $\mathcal{H}_\infty$ norms for aggregate output, and even 83% of the worst-case cross-sectional amplification. Only when we drop to 21 sectors or less do we see notable decay in retention.

The $\mathcal{H}_2$ norm retention results also provide an orthogonal decomposition of the share of the detailed-sector variance due to shocks at different levels of aggregation. Because the admissible shock spaces are nested, their increments are orthogonal, making the squared $\mathcal{H}_2$ norms are additive. For example, an aggregate shock common to all sectors retains 43.9% of the detailed $\mathcal{H}_2$ norm, which means that $0.439^2 = 19.3\%$ of aggregate variance in the detailed network is driven by aggregate shocks. The retention ratio increases to 0.754 at the 21-sector level, so the share of variance accounted for by 21-sector variation orthogonal to the common aggregate shock is $0.754^2 - 0.439^2 = 37.5\%$. Thus 82% of the aggregate output variance is accounted for by shocks at the 71-sector level or coarser.

These results justify the time-series analysis in the next section. The 71-sector panel, which is available in a consistent annual panel, is fine enough to capture the main structure of the detailed network, particularly in its implications for aggregate output. Most of the volatility and fragility in the detailed industry-level input-output network comes from shocks and uncertainty at the 71-sector or coarser levels of aggregation.

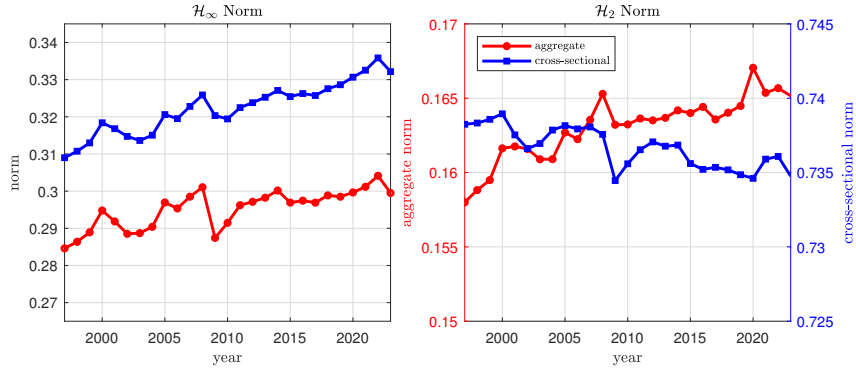


FIGURE 6. Time series of fragility ($\mathcal{H}_\infty$) and volatility ($\mathcal{H}_2$) for aggregate and cross-sectional output in the 71-sector US production network.

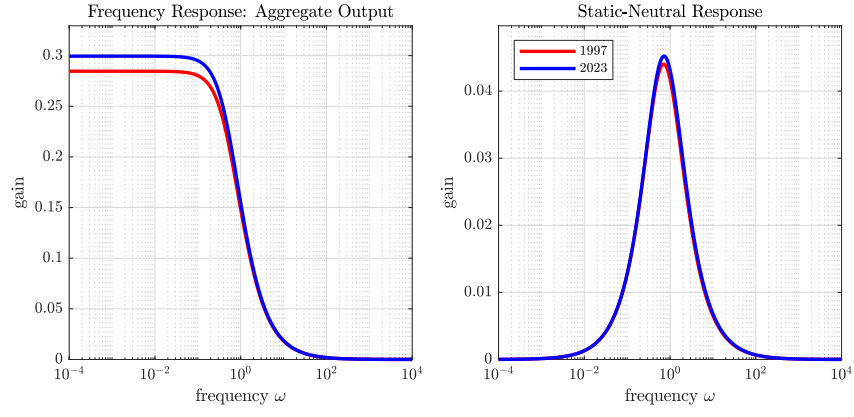


FIGURE 7. Frequency responses for aggregate output in 1997 and 2023. Left panel: unrestricted. Right panel: static-neutral.

6.2 *Changes in the US Production Network*

I now study how the US production network has changed over time, using the annual 71-sector panel from 1997 to 2023. Figure 6 plots the time series of cross-sectional and aggregate metrics. There has been a mild increase in fragility, as the $\mathcal{H}_\infty$ norm has increased by 5.2% for aggregate output and 7.5% for cross-sectional output over the sample period. Aggregate volatility, as measured by the $\mathcal{H}_2$ norm, has also increased by 4.5%, while cross-sectional volatility has been roughly constant, with a 0.5% decline. By comparison, Appendix C.4 shows that all of these metrics decline over time, to varying degrees, for the more aggregated 21-sector network. Too much aggregation may mask volatility in the network, as reallocation within a broader sector dampens fragility to finer shocks.

Figure 7 plots the frequency responses for aggregate output in 1997 and 2023, showing both the baseline unrestricted case and the static-neutral response. The baseline response shows a notable, but mild, increase over time for low frequencies. The increase

TABLE 2. Top 2023 aggregate worst-case input components, with 1997 for comparison.

		2023				1997			
Rank	Sector	Energy	ν_i	s_i	Total	Energy	ν_i	s_i	Total
1	Misc prof, sci, and tech services	18.7%	6.3%	2.149	0.056	15.7%	5.2%	2.327	0.045
2	Wholesale trade	11.2%	5.8%	2.304	0.034	12.2%	6.1%	1.774	0.035
3	Housing	9.9%	9.4%	0.000	0.030	9.3%	8.7%	0.000	0.027
4	Other real estate	9.7%	2.9%	2.269	0.029	4.3%	1.9%	1.551	0.012
5	Administrative & support services	6.2%	2.9%	1.565	0.019	4.2%	2.3%	1.434	0.012
6	State and local general government	4.7%	6.5%	0.000	0.014	7.0%	7.5%	0.000	0.020
7	Federal Reserve banks, credit intermed	4.6%	3.3%	1.091	0.014	3.4%	2.7%	0.763	0.010
8	Insurance carriers & related activities	4.5%	2.6%	1.137	0.014	2.8%	2.5%	0.833	0.008
9	Construction	4.1%	4.9%	0.541	0.012	3.8%	4.5%	0.450	0.011
10	Chemical products	2.4%	1.7%	1.419	0.007	3.6%	1.8%	1.462	0.010

in the peak at frequency zero and increased area under the curve indicate that both $\mathcal{H}_\infty$ and $\mathcal{H}_2$ increased over time. The right panel shows that the static-neutral responses are notably smaller, with a gain of roughly 15% of the unrestricted case, quite similar across years. The peak static-neutral response occurs at $\omega^* = 0.726$, so the relevant oscillations have a period of about 8.7 years.

Table 2 provides a diagnosis of the worst-case input direction in the 71-sector network, and how it has changed from 1997 to 2023. The table reports the top ten sectors from 2023 in terms of the energy share of the worst-case input $\bar{v}$, the sector's GDP weight ν_i and supplier strength s_i, along with the total long-run impact of the shock $(\nu^\top L^{-1})_i \bar{v}_i$. Similar to the detailed network, the worst-case input loads heavily on housing and other real estate, service employment, financial industries, and state and local government. But at this more aggregated level, some new sectors become more important. The top two sectors, miscellaneous professional, scientific, and technical services and wholesale trade, aggregate ten or eleven industries from the 398-sector network. While the detailed industries were relatively small, the aggregated sectors each account for around 6% of GDP and have supplier strengths exceeding 2, meaning their outputs are heavily used as inputs into other sectors. Overall, the worst-case input is again a service-sector, real-estate, and financial recession.

Table 2 also reports the values of the indicators for these sectors in 1997. At the earlier date, the top sectors in the aggregate worst-case input were similar, but some of the values and relative rankings changed over time. Over time, the worst-case input vector has become more concentrated in real estate and services. The largest changes came in the other real estate sector, comprising commercial and non-residential real estate. From 1997 to 2023 its GDP share grew by one percentage point and its supplier strength increased by almost 50%, resulting in its energy share increasing from 4.3% to 9.7%. Similar increases of smaller magnitude occurred for service-sector employment sectors (at ranks 1 and 5). Since the late 1990s the US production network became more heavily reliant on real estate and service-sector employment. In addition, commercial real estate, wholesale trade and distribution, and financial services broadly (including credit and insurance) became more important as suppliers to other sectors. Since aggregate

TABLE 3. Changes in the 71-sector network

Diagnostic	1997	2023	Change	Diagnostic	1997	2023	Change
Mean intermediate β_i	0.466	0.454	-2.6%	Std dev s_i	0.475	0.524	+10.3%
Std dev β_i	0.160	0.144	-9.8%	Supplier s_i eff N	15.079	12.039	-20.2%
A spectral radius	0.482	0.467	-3.2%	Aggregate $\bar{v}$ top 5 share	0.486	0.558	+14.8%
$\bar{\sigma}(L^{-1})$ singular value	2.287	2.282	-0.2%	Aggregate $\bar{v}$ eff N	14.937	12.181	-18.4%
GDP-share ν_i eff N	9.145	8.999	-1.6%	Cross-sec $\bar{v}$ top 5 share	0.717	0.788	+9.9%
GDP-share ν_i std dev	0.016	0.017	+4.5%	Cross-sec $\bar{v}$ eff N	6.595	4.307	-34.7%

output is now more sensitive to fluctuations in these key sectors, both directly through an increased GDP share and indirectly through their roles as suppliers, the worst-case input concentrates its energy there.

Table 3 provides summary statistics that detail changes in network components and the worst-case shock vectors between 1997 and 2023. These results highlight that the increased fragility and volatility are driven by changes in the concentration of economic activity, and that these effects crucially depend on the asymmetry of the production network. In symmetric networks, the intermediate share β_i is equal to the supplier strength s_i, but these measures clearly behave differently in the production network. Their means are equal by definition, and thus both experienced a slight decline over time. The intermediate share distribution became notably more compressed, as sectors became more similar in their use of inputs. However, the supplier strength distribution grew more dispersed and concentrated. A few sectors saw a notable increase in their sales to other sectors, while most had a slight decline in their uses as inputs. Overall, this reflects the continuing decline in goods-producing sectors, and the growth of services, distribution, and FIRE (finance, insurance, and real estate) both as final goods and as inputs.

The table also shows how these asymmetries and concentration manifest in shock propagation through the network. Standard spectral measures would not suggest increased fragility, as the production network did not move closer to the instability region. The spectral radius of the network adjacency matrix and the maximal singular value of the Leontief inverse both decline slightly. Instead, the fragility comes from the increased concentration of supplier activity. The worst-case shock vector reflects this concentration, pooling most of its energy in a few key sectors. While I have focused mainly on aggregate output, the concentration is especially strong in cross-sectional output, where shocks to a few key sectors drive most of the cross-sectional fragility.

6.3 *Static-Neutral Shocks*

Figure 8 shows the cyclical time paths of the leading sectors in the worst-case static-neutral input. The input vector, whose numerical values and energy shares are provided in Appendix C.5, is very concentrated. The top five sectors account for 67.1% of input energy, and the top ten account for 84.2%. The sectors fall in two nearly opposite phase blocks. Housing, state and local government, and health care are the largest positive-phase components, shown in Figure 8 with solid lines. Not shown are the smaller positive contributions from construction and retail. The leading sectors that load on the

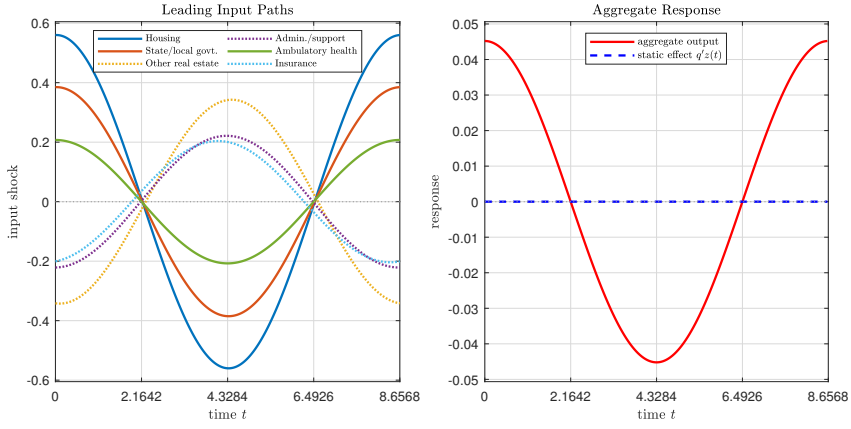


FIGURE 8. Worst-case static-neutral shocks in the 2023 71-sector network. Left panel: cyclical time paths of leading sectoral input components. Right panel: aggregate response, with the dashed line showing the zero static aggregate effect.

opposite phase are other real estate, administrative and support services, and insurance, shown in Figure 8 with dashed lines. Not shown are the smaller contributions from chemicals and primary metals. The sectoral fluctuations are an order of magnitude larger than their aggregate, with the shocks cycling between the two blocks. The right panel shows that these sectoral responses contribute to a cycle in aggregate output, while the static response remains at zero.

This illustrates that the US production network is susceptible to dynamic sectoral reallocations of economic activity that are by construction not detectable in a static setting. One block consists of sectors tied to household services and residential demand, which are important in final expenditure but matter less as inputs in other sectors. (Recall the supplier strengths for housing and state and local government services are zero.) The other block consists of sectors that are more important as inputs in production, such as commercial real estate, business services, and insurance. The shock cycles activity between final-demand-intensive sectors and sectors with greater downstream exposure. Since the two blocks differ in their propagation through the network, the reallocation produces aggregate fluctuations.

7. CONCLUSION

This paper develops an approach to evaluate the performance and robustness of dynamics on networks using concepts from control theory. I study two common measures of performance: the $\mathcal{H}_2$ norm summarizing average volatility generated by stochastic shocks, and the $\mathcal{H}_\infty$ norm capturing worst-case amplification and robustness. I develop frequency-domain methods that separate impacts driven by low-frequency disturbances due to persistent biases from vulnerabilities that arise at interior frequencies through propagation and feedback. I show how in normal or undirected networks components of the network spectrum govern the performance measures, while also illustrating how these measures change when networks are directed and flows are asymmetric. I

apply the methods here to analyze production networks, and in Williams (2026) I study information networks.

I develop several examples that can be solved explicitly, illustrating how connectedness, redundancy, and speeds of adjustment affect the network dynamics. Across the examples, performance and robustness depend on the distribution of local "leakages" or restoring forces and where bottlenecks lie in the network. When networks are directed and non-normal, the dynamics separate upstream and downstream nodes, and can generate large amplification even when eigenvalue-based measures suggest strong stability.

Then I study the production network in the United States. I find that most of the sources of volatility and fragility come from shocks and uncertainty at the sectoral or coarser levels of aggregation. The most damaging shock vector is concentrated in services, real estate, and finance, then propagates to the rest of the economy. Over the past 25 years, the US economy has become more fragile and subject to aggregate output volatility coming through the production network. This is driven by two main factors: (1) the increased concentration of economic activity in services and real estate, so shocks to these sectors now have a larger direct effect on aggregate output, and (2) the increased importance of finance and real estate as inputs across many different sectors, so the total effect of shocks is magnified as the shocks propagate through the production network.

As mentioned above, this paper focuses on analysis rather than synthesis, in that I take as given the network structure. But the methods here could be tools to study network control and design. One direction is to directly study decisions or policies that alter diffusion or routing in order to improve performance and robustness, trading off stabilization benefits against intervention costs. A complementary direction is network design, characterizing the performance benefits of adding or reweighting links compared to the costs of link formation and maintenance. These problems connect the positive analysis of propagation to normative questions about optimal resilience and the architecture of networks.

References

Acemoglu, D. and P. D. Azar (2020). Endogenous production networks. *Econometrica 88*(1), 33–82. [2]

Acemoglu, D., V. M. Carvalho, A. Ozdaglar, and A. Tahbaz-Salehi (2012). The network origins of aggregate fluctuations. *Econometrica 80*(5), 1977–2016. [2, 49, 51]

Atalay, E. (2017). How important are sectoral shocks? *American Economic Journal: Macroeconomics 9*(4), 254–280. [2]

Ballester, C., A. Calvó-Armengol, and Y. Zenou (2006). Who's who in networks. Wanted: The key player. *Econometrica 74*(5), 1403–1417. [3]

Baqaee, D. (2018). Cascading failures in production networks. *Econometrica 86*(5), 1819–1838. [2]

Baqaee, D. and E. Farhi (2019). The macroeconomic impact of microeconomic shocks: Beyond Hulten's theorem. *Econometrica 87*(3), 1155–1203. [2]

Baqaee, D. and E. Farhi (2020). Productivity and welfare measurement with production networks. *Econometrica 88*(5), 2039–2066. [2]

Bloch, F., M. O. Jackson, and P. Tebaldi (2023). Centrality measures in networks. *Social Choice and Welfare 61*(2), 413–453. [3]

Boehm, C. E., A. Flaaen, and N. Pandalai-Nayar (2019). Input linkages and the transmission of shocks: Firm-level evidence from the 2011 Tōhoku earthquake. *Review of Economics and Statistics 101*(1), 60–75. [2]

Bonacich, P. (1987). Power and centrality: A family of measures. *American Journal of Sociology 92*(5), 1170–1182. [3]

Boyd, S., P. Diaconis, P. Parrilo, and L. Xiao (2005). Symmetry analysis of reversible Markov chains. *Internet Mathematics 2*(1), 31–71. [43]

Brock, W. A. and S. N. Durlauf (2005). Local robustness analysis: Theory and application. *Journal of Economic Dynamics and Control 29*(11), 2067–2092. [3]

Brock, W. A., S. N. Durlauf, and G. Rondina (2013). Design limits and dynamic policy analysis. *Journal of Economic Dynamics and Control 37*(12), 2710–2728. [3]

Brouwer, A. E. and W. H. Haemers (2012). *Spectra of Graphs*. Universitext. New York, NY: Springer. [43]

Carvalho, V. M., M. Covarrubias, and G. Nuño (2025). Planning against disasters in dynamic production networks. Working paper. [2]

Carvalho, V. M. and A. Tahbaz-Salehi (2019). Production networks: A primer. *Annual Review of Economics 11*, 635–663. [2, 5, 14]

DeGroot, M. H. (1974). Reaching a consensus. *Journal of the American Statistical Association 69*(345), 118–121. [4, 6]

Dupor, W. (1999). Aggregation and irrelevance in multi-sector models. *Journal of Monetary Economics 43*(2), 391–409. [2]

Elliott, M., B. Golub, and M. V. Leduc (2022). Supply network formation and fragility. *American Economic Review 112*(8), 2701–2747. [2]

Elliott, M. and M. O. Jackson (2026). Supply chain disruptions, the structure of production networks, and the impact of globalization. Working paper. [2]

Foerster, A. T., P.-D. G. Sarte, and M. W. Watson (2011). Sectoral versus aggregate shocks: A structural factor analysis of industrial production. *Journal of Political Economy 119*(1), 1–38. [2]

Gabaix, X. (2011). The granular origins of aggregate fluctuations. *Econometrica 79*(3), 733–772. [2]

Golub, B. and M. O. Jackson (2010). Naïve learning in social networks and the wisdom of crowds. *American Economic Journal: Microeconomics 2*(1), 112–149. [6]

Goyal, S. (2023). *Networks: An Economics Approach*. Cambridge, MA: MIT Press. [1]

Gray, R. M. (2006). Toeplitz and circulant matrices: A review. *Foundations and Trends in Communications and Information Theory 2*(3), 155–239. [47]

Hansen, L. P. and T. J. Sargent (2008). *Robustness*. Princeton, NJ: Princeton University Press. [3, 9, 37]

Horn, R. A. and C. R. Johnson (2013). *Matrix Analysis* (Second ed.). Cambridge: Cambridge University Press. [42]

Horvath, M. (1998). Cyclicality and sectoral linkages: Aggregate fluctuations from sectoral shocks. *Review of Economic Dynamics 1*(4), 781–808. [2]

Huo, Z., A. A. Levchenko, and N. Pandalai-Nayar (2025). International comovement in the global production network. *Review of Economic Studies 92*(1), 365–403. [2]

Jackson, M. O. (2008). *Social and Economic Networks*. Princeton, NJ: Princeton University Press. [1, 6]

Katz, L. (1953). A new status index derived from sociometric analysis. *Psychometrika 18*(1), 39–43. [3]

Kopytov, A., B. Mishra, K. Nimark, and M. Taschereau-Dumouchel (2024). Endogenous production networks under supply chain uncertainty. *Econometrica 92*(5), 1621–1659. [2]

Lancaster, P. and M. Tismenetsky (1985). *The Theory of Matrices* (2 ed.). Academic Press. [12]

Liu, E. and A. Tsyvinski (2024). A dynamic model of input–output networks. *Review of Economic Studies 91*(6), 3608–3644. [2]

Long, J. B. J. and C. I. Plosser (1983). Real business cycles. *Journal of Political Economy 91*(1), 39–69. [2, 4]

Newman, M. E. J. (2018). *Networks* (2 ed.). Oxford: Oxford University Press. [2]

Onatski, A. and N. Williams (2003). Modeling model uncertainty. *Journal of the European Economic Association 1*(5), 1087–1122. [3, 16]

Pass, R. (2019). *A Course in Networks and Markets: Game-theoretic Models and Reasoning*. Cambridge, MA: MIT Press. [1]

Rantzer, A. (2012). Distributed control of positive systems. *Proceedings of the IFAC World Congress 45*(26), 492–497. [12, 40]

Schaal, E. and M. Taschereau-Dumouchel (2025). Echoes and delays: Time-to-build in production networks. Working paper. [2]

Skogestad, S. and I. Postlethwaite (2005). *Multivariable Feedback Control: Analysis and Design* (2 ed.). Chichester: John Wiley & Sons. [3, 6, 10]

Taschereau-Dumouchel, M. (2025). Cascades and fluctuations in an economy with an endogenous production network. *The Review of Economic Studies*, forthcoming. [2]

U.S. Bureau of Economic Analysis (2026). Input-Output Accounts and Input-Output Interactive Data Tables. U.S. Department of Commerce. [4, 26, 49, 51]

Van Mieghem, P. (2023). *Graph Spectra for Complex Networks* (2 ed.). Cambridge: Cambridge University Press. [2, 41, 43, 47]

Veerman, J. J. P. and R. Lyons (2020). A primer on Laplacian dynamics in directed graphs. *Nonlinear Phenomena in Complex Systems 23*(2), 199–216. [2]

vom Lehn, C. and T. Winberry (2022). The investment network, sectoral comovement, and the changing U.S. business cycle. *The Quarterly Journal of Economics 137*(1), 387–433. [2]

Williams, N. (2026). Disagreement in information networks. Working paper. [2, 4, 6, 33]

Yadykin, A. and A. Iskakov (2021). Modal analysis of the Sylvester equation via orthogonal decompositions. *Automatica 131*, 109748. [11, 40]

Zhou, K. and J. C. Doyle (1998). *Essentials of Robust Control*. Upper Saddle River, NJ: Prentice Hall. [3]

Zhou, K., J. C. Doyle, and K. Glover (1996). *Robust and Optimal Control*. Upper Saddle River, NJ: Prentice Hall. [3, 10, 37, 38]

APPENDIX A: EXTENSIONS AND PROOFS

A.1 *More Detail on the Long and Plosser Model*

The production side of the model was laid out in the main text. On the demand side, a representative consumer chooses labor supply and consumption to maximize utility. Preferences are separable and logarithmic over leisure ℓ_t and the vector of consumptions $C_t = \{C_{i,t}\}$ across goods:

$$U(C_t, \ell_t) = \theta_0 \log \ell_t + \sum_{i=1}^{N} \theta_i \log C_{i,t},$$

where the weights θ_0 and θ_i capture the importance of leisure and each good in utility. The time constraint requires that leisure plus total labor supplied across sectors equals a fixed time endowment h:

$$\ell_t + \sum_{i=1}^{N} L_{i,t} = h.$$

Markets clear each period: the output of each sector equals the sum of its consumption and use as an intermediate input by other sectors,

$$Y_{j,t} = C_{j,t} + \sum_{i=1}^{N} X_{ij,t}.$$

Under these conditions, equilibrium allocations can be solved explicitly. The allocation of labor across sectors is constant at $L_{i,t} = \bar{L}_i$, and consumers choose a constant level of

leisure $\ell_t = \bar{\ell}$. Intermediate inputs are demanded in fixed proportions of output, so that $X_{ij,t} = \bar{x}_{ij} Y_{j,t}$ for some constants $\bar{x}_{ij}$.

Substituting these relationships into the production function and taking logarithms yields a dynamic linear equation for output. The log of sectoral output evolves as:

$$\log Y_{i,t+1} = k_i + \sum_{j=1}^{N} a_{ij} \log Y_{j,t} + \log Z_{i,t+1},$$

where k_i is a constant and a_{ij} is the share of good j used by sector i in production. Vectorizing and using the notation in the text gives:

$$x_{t+1} = Ax_t + z_{t+1} \Rightarrow x_{t+1} - x_t = (A - \mathrm{I})x_t + z_{t+1}.$$

The continuous-time system is the natural Euler embedding of this discrete-time system.

A.2 *Modeling Uncertainty*

A general and flexible approach to modeling uncertainty is to represent misspecification as a feedback distortion of the effective disturbance entering the model. We begin with a baseline nominal model:

$$y(s) = G(s)u_0(s), \qquad G(s) = C(sI - M)^{-1}B, \tag{17}$$

where u_0 denotes the primitive shocks under the nominal model.[25] The true model is unknown and may differ from (17) in its parameters, structure, or measurement relationships. Rather than attempting to model these deviations explicitly, I represent their effect as a distortion of the disturbance entering the nominal dynamics. Specifically, I adopt the feedback representation given in (5). The unknown but stable and norm-bounded perturbation $\Delta(s)$ captures deviations from the nominal model, so the input $u(s) = u_0(s) + \Delta(s)y(s)$ is a combination of shocks to the nominal model $u_0(s)$ and the uncertainty $\Delta(s)$.

This formulation captures a wide class of possible deviations from the nominal model. In particular, several common sources of uncertainty can be embedded in, or bounded by, a representation of the form (5).

1. **Uncertainty in network structure or dynamics.** Suppose the true system matrix differs from the nominal one,

   $$M = M_0 + \Delta_M,$$

   where Δ_M is unknown but bounded. The true dynamics are

   $$\dot{x} = (M_0 + \Delta_M)x + Bu_0.$$

[25] The nominal model in control theory, for example Zhou, Doyle, and Glover (1996), is also called the approximating model in economics, as in Hansen and Sargent (2008).

This can be written exactly as

$$\dot{x} = M_0 x + B u_0 + \Delta_M x.$$

In the frequency domain, this corresponds to a feedback operator acting on the state x. But since x and y are related by the nominal dynamics, this state-feedback uncertainty can often be embedded, or conservatively represented, in the form (5). Uncertainty in the network thus induces a feedback distortion of the effective disturbance entering the nominal model.

2. **Input-channel uncertainty.** Suppose that shocks are distorted before entering the system, so that the actual disturbance is

$$u = u_0 + \tilde{u},$$

where $\tilde{u}$ captures both mismeasurement of shocks and misspecification of how they propagate through the system. If the distortion depends on current or past outcomes, for example, because agents infer shocks from observed activity, then the distortion can be modeled as $\tilde{u} = \Delta y$, leading directly to the feedback structure (5). Even when such dependence is not modeled explicitly, bounding the effect of input distortion by a norm constraint on Δ provides a conservative but tractable robustness measure.

3. **Output-side uncertainty.** If the reported output differs from the true output, for example due to aggregation bias or delayed measurement, then

$$\tilde{y} = y + \Delta_y y.$$

Since the effective disturbance entering decision rules or subsequent dynamics depends on observed outcomes, such output-side distortions again induce feedback effects. Under mild regularity conditions, these effects can be absorbed into a representation of the form (5). When an exact embedding is not possible, the feedback formulation still provides an upper bound on the induced distortion.

These examples illustrate that a broad class of model uncertainties can be represented, exactly or conservatively, as norm-bounded feedback distortions of the effective disturbance. This representation allows for robustness analysis using the $\mathcal{H}_\infty$ norm of the nominal transfer function, without committing to a specific structure of misspecification.

A.3 *Proof of Theorem 1*

This proof sketch of the Small Gain Theorem follows Zhou, Doyle, and Glover (1996), and allows for complex perturbations.

PROOF. Using (5), write $u = u_0 + \Delta y$ and $y = Gu$, so that

$$(\mathrm{I} - G\Delta)y = Gu_0, \qquad (\mathrm{I} - \Delta G)u = u_0.$$

Since G and Δ are both stable, it is enough to show that the return-difference inverses $(\mathrm{I}-G\Delta)^{-1}$ and $(\mathrm{I}-\Delta G)^{-1}$ belong to $\mathcal{H}_\infty$.

For sufficiency, suppose $\|G\|_\infty \le \gamma$ and $\|\Delta\|_\infty < 1/\gamma$. Then by submultiplicativity of the induced norm,

$$\|G\Delta\|_\infty \le \|G\|_\infty \|\Delta\|_\infty < 1, \qquad \|\Delta G\|_\infty \le \|\Delta\|_\infty \|G\|_\infty < 1.$$

Hence the geometric series converge in $\mathcal{H}_\infty$:

$$(\mathrm{I}-G\Delta)^{-1} = \sum_{k=0}^{\infty} (G\Delta)^k, \qquad (\mathrm{I}-\Delta G)^{-1} = \sum_{k=0}^{\infty} (\Delta G)^k.$$

Therefore

$$y = (\mathrm{I}-G\Delta)^{-1} G u_0, \qquad u = (\mathrm{I}-\Delta G)^{-1} u_0$$

are stable transfer functions of u_0. Thus the feedback interconnection is internally stable for every Δ satisfying $\|\Delta\|_\infty < 1/\gamma$.

For necessity, argue by contrapositive. Suppose that $\|G\|_\infty > \gamma$. Then there exists some $\omega_\star \in \mathbb{R}$ such that

$$\sigma_\star = \bar{\sigma}\big(G(j\omega_\star)\big) > \gamma.$$

Let $x_\star$ and $z_\star$ be unit left and right singular vectors associated with $\sigma_\star$, so

$$G(j\omega_\star) z_\star = \sigma_\star x_\star, \qquad G(j\omega_\star)^H x_\star = \sigma_\star z_\star.$$

Now define the static rank-one perturbation

$$\Delta_0(s) \equiv \Delta_0 = \frac{1}{\sigma_\star} z_\star x_\star^H.$$

Then Δ_0 is stable, $\Delta_0 \in \mathcal{H}_\infty$, and

$$\|\Delta_0\|_\infty = \|\Delta_0\| = \frac{1}{\sigma_\star} < \frac{1}{\gamma}.$$

Moreover,

$$G(j\omega_\star)\Delta_0 x_\star = G(j\omega_\star)\frac{1}{\sigma_\star} z_\star (x_\star^H x_\star) = x_\star,$$

so

$$(\mathrm{I} - G(j\omega_\star)\Delta_0) x_\star = 0.$$

Thus $\mathrm{I} - G(j\omega_\star)\Delta_0$ is singular. By continuity, the norm of $(\mathrm{I}-G(j\omega)\Delta_0)^{-1}$ becomes arbitrarily large as $\omega \to \omega_\star$, so $(\mathrm{I}-G\Delta_0)^{-1} \notin \mathcal{H}_\infty$. Hence the feedback interconnection is not internally stable.

At the frequency $\omega_\star$, the system maps the input direction $z_\star$ into the output direction $x_\star$ with gain $\sigma_\star$. The perturbation Δ_0 feeds that output direction back into the same dangerous input direction with gain $1/\sigma_\star$, so the round-trip gain is exactly one. $\square$

A.4 *Proof of Theorem 2.*

PROOF. The proof follows standard calculations. When $u(t)$ is Gaussian white noise, we can define $P(t) = E(x(t)x(t)^H)$. Then we have the dynamics:

$$\dot{P} = MP + PM^H + BB^H,$$

and hence the Lyapunov equation gives the steady-state value of P. Since $y(t) = Cx(t)$, then $E(y(t)y(t)^H) = CPC^H$, and hence

$$\|G\|_2^2 = E(y(t)^H y(t)) = \mathrm{tr}(CPC^H).$$

□

A.5 *Proof of Theorem 3*

PROOF. The expression for Y_{ij} is a special case of the block–modal representation of solutions to the Lyapunov equation in Yadykin and Iskakov (2021) for diagonalizable systems. The additional matrix S_e enters when computing the $\mathcal{H}_2$ norm via the trace identity. Explicitly, using the results above the $\mathcal{H}_2$ norm is

$$\|G\|_2^2 = \mathrm{tr}(CPC^H) = \mathrm{tr}\big(CVYV^HC^H\big) = \mathrm{tr}\big(S_eY\big),$$

where the last equality uses the cyclicality of the trace and the definition of S_e. Then expanding the terms in the trace we have:

$$\|G\|_2^2 = \mathrm{tr}\big(S_eY\big) = \sum_{i,j} S_{e,ji}Y_{ij} = \sum_{i,j} \frac{S_{e,ji}B_{e,ij}}{\lambda_i + \overline{\lambda_j}}.$$

□

A.6 *Proof of Theorem 4*

PROOF. This proof follows Rantzer (2012), adapted to my setting. Because $A \geq 0$ with row sums < 1, all eigenvalues of $L = I - A$ satisfy $\Re\lambda_i(L) > 0$ and $-L$ is Metzler. Hence e^{-Lt} is entry-wise nonnegative for all $t \geq 0$. With $B, C \geq 0$, the impulse response

$$h(t) \;=\; Ce^{-Lt}B$$

is also entry-wise nonnegative. The transfer function is its Laplace transform

$$G(j\omega) = \int_0^\infty e^{-j\omega t}h(t)\,dt.$$

For each entry (k,ℓ) of $G(j\omega)$ we have

$$\big|G_{k\ell}(j\omega)\big| = \Big|\int_0^\infty e^{-j\omega t}\,h_{k\ell}(t)\,dt\Big| \leq \int_0^\infty |e^{-j\omega t}|\,h_{k\ell}(t)\,dt = \int_0^\infty h_{k\ell}(t)\,dt \;=\; G_{k\ell}(0).$$

Hence the matrices satisfy the entry-wise inequality

$$|G(j\omega)| \;\le\; G(0).$$

For any matrix M, the spectral norm obeys $\|M\|_2 \le \||M|\|_2$, and if $0 \le X \le Y$ entry-wise with $Y \ge 0$, then $\|X\|_2 \le \|Y\|_2$. Applying these facts to $X = |G(j\omega)|$ and $Y = G(0)$ gives

$$\|G(j\omega)\|_2 \;\le\; \big\||G(j\omega)|\big\|_2 \;\le\; \|G(0)\|_2 \qquad \forall\, \omega \in \mathbb{R}.$$

Since equality holds at $\omega = 0$, we conclude

$$\sup_{\omega\in\mathbb{R}} \|G(j\omega)\|_2 = \|G(0)\|_2 = \Big\| \int_0^\infty h(t)\, dt \Big\|_2 = \|CL^{-1}B\|_2.$$

□

A.7 *Proof of Proposition 1*

PROOF. As noted in the text, by construction we have

$$G_{\mathcal{S}}(0) = c^\top L^{-1} B_{\mathcal{S}} = q^\top B_{\mathcal{S}} = 0.$$

Since L is stable,

$$(j\omega I + L)^{-1} \to 0 \qquad \text{as} \qquad |\omega| \to \infty,$$

and therefore $G_{\mathcal{S}}(j\omega) \to 0$. The function $\|G_{\mathcal{S}}(j\omega)\|_2$ is continuous in ω. If $G_{\mathcal{S}}$ is not identically zero, it is positive at some frequency, equals zero at $\omega = 0$, and tends to zero at infinity. Its maximum is therefore attained at some finite frequency with $|\omega^*| > 0$. □

APPENDIX B: ADDITIONAL EXAMPLES AND DETAILED CALCULATIONS

B.1 *Complete Network*

I start with additional examples and calculations for the complete network in Section 5.1.2. The baseline adjacency matrix is

$$A_0 = \frac{1}{N} 1_N 1_N^\top.$$

The baseline Laplacian $L_0 = I - A_0$ then has eigenvalues $\lambda_1 = 0$, $\lambda_2 = \cdots = \lambda_N = 1$.[26]

B.1.1 *Production Networks: Cross-Section* For production networks, we start with cross-sectional output $C = I$ and homogeneous intermediate shares β. The text provides a brief description, using that $L = I - \beta A_0 = (1-\beta)I + \beta L_0$, so its eigenvalues follow from those of L_0.

Introducing heterogeneous shares using the approach in the text, the Laplacian becomes:

$$L = I - \beta A_0 - \Gamma = D - \beta A_0 = D - \frac{\beta}{N} 1_N 1_N^\top.$$

[26] Van Mieghem (2023) provides related results under a slightly different normalization of the graph.

With heterogeneous labor shares, the complete network can be decomposed into a uniform mixing provided by the network, along with different degrees of persistence in each sector. Mathematically, L is composed of a diagonal matrix D plus a rank-one perturbation, so its inverse follows directly from the Sherman–Morrison-Woodbury formula[27]

$$L^{-1} = D^{-1} + \frac{\beta}{\eta N} D^{-1} 1_N 1_N^\top D^{-1}.$$

Using the structure of d and s_1 and s_2 as defined in the text, this gives:

$$\|G\|_2^2 = \frac{1}{2}\operatorname{tr}(L^{-1}) = \frac{1}{2}\left(s_1 + \frac{\beta}{\eta N} s_2\right).$$

Recall that $d_i = 1 - \beta_i + \beta$, and define the following:

$$s_1 = \sum_{i=1}^N \frac{1}{d_i}, \qquad s_2 = \sum_{i=1}^N \frac{1}{d_i^2}, \qquad \eta = 1 - \frac{\beta}{N} s_1.$$

A small intermediate share β_i means a large d_i and more rapid adjustment in that sector.

For worst-case analysis, we must find the minimal eigenvalue of L, which is no longer directly related to that of L_0. For $\lambda \notin \{d_1, \ldots, d_N\}$, we write the characteristic equation using the matrix determinant lemma:

$$\det(L - \lambda I) = \det\Big(D - \lambda I - \frac{\beta}{N} 1_N 1_N^\top\Big) = \det(D - \lambda I)\, \det\Big(I - \frac{\beta}{N}(D - \lambda I)^{-1} 1_N 1_N^\top\Big).$$

Since $1_N 1_N^\top$ is rank one,

$$\det\Big(I - \frac{\beta}{N}(D - \lambda I)^{-1} 1_N 1_N^\top\Big) = 1 - \frac{\beta}{N} 1_N^\top (D - \lambda I)^{-1} 1_N = 1 - \frac{\beta}{N} \sum_{i=1}^N \frac{1}{d_i - \lambda}.$$

Hence the eigenvalues are given by the roots of equation (16) in the text, together with any eigenvalues $\lambda_i = d_i$ that may arise from eigenvectors orthogonal to 1_N. The corresponding eigenvector has an explicit componentwise form. From $(L - \lambda I)v = 0$ we have

$$(D - \lambda I)v = \frac{\beta}{N} 1_N (1_N^\top v).$$

so $\overline{v}_i = \frac{v_0}{d_i - \underline{\lambda}}$ for some constant $v_0 \neq 0$.

B.1.2 *Production Networks: Aggregate Output* With homogeneous intermediate shares $\beta_i = \beta$, both performance measures collapse to values independent of the network structure. But that is no longer the case with heterogeneous labor shares. Using $L^{-1} 1_N = \frac{1}{\eta} D^{-1} 1_N$, we have from the calculations above:

$$1_N^\top L^{-1} 1_N = 1_N^\top D^{-1} 1_N + \frac{\beta}{\eta N} (1_N^\top D^{-1} 1_N)^2 = s_1 + \frac{\beta}{\eta N} s_1^2.$$

[27] See Horn and Johnson (2013), p. 19.

Thus using the result (12) above:

$$\|G\|_2^2 = \frac{1}{2}\, 1_N^\top L^{-1} 1_N = \frac{1}{2}\left(s_1 + \frac{\beta}{\eta N}\, s_1^2\right).$$

This is similar to the cross-sectional $\mathcal{H}_2$ norm above, but now the second component has s_1^2 instead of s_2, reflecting that here we aggregate before computing volatility.

Similarly, from (13) above we have:

$$\|G\|_\infty = \|L^{-1}1_N\|_2 = \frac{1}{\eta}\|D^{-1}1_N\|_2 = \frac{\sqrt{s_2}}{\eta}.$$

This expression is quite similar to what we had with uniform labor shares, $\sqrt{N}/(1-\beta)$. Now with heterogeneity, η rather than $1-\beta$ measures the effective stability margin, incorporating the different sectoral adjustment speeds. Similarly, $\sqrt{s_2}$ measures the size of the sectoral persistence weights, which collapses to $\sqrt{N}$ in the homogeneous case. Moreover, the worst-case input now has the explicit expression:

$$\overline{v} \propto L^{-1}1_N \propto D^{-1}1_N, \quad \text{so: } \overline{v}_i \propto \frac{1}{d_i}.$$

The most damaging disturbance for aggregate output concentrates on slow-adjusting, low labor share (low d_i) sectors. Since in this example sectoral connections are all complete and symmetric, aggregate robustness is governed by sectoral bottlenecks.

B.2 *Path Graph*

Let A_0 be the path, or symmetric reflecting random walk on $\{1,\dots,N\}$,

$$(A_0)_{ij} = \begin{cases} \frac{1}{2}, & |i-j| = 1, \\ \frac{1}{2}, & i = j \in \{1, N\}, \\ 0, & \text{otherwise}, \end{cases} \qquad i,j = 1,\dots,N.$$

The eigenvalues of the baseline Laplacian $L_0 = I - A_0$ are given by [28]:

$$\lambda_i = 1 - \cos\Big(\frac{(i-1)\pi}{N}\Big), \qquad i = 1,\dots,N,$$

so $\lambda_1 = 0$ and the algebraic connectivity satisfies:

$$\lambda_2 = 1 - \cos\left(\frac{\pi}{N}\right) \sim \frac{\pi^2}{2N^2} \text{ as } N \to \infty.$$

Thus the path network has very low connectivity for large N, scaling like N^{-2}, in comparison to the complete network which was constant.

[28] The cosine spectrum and eigenfunctions for the double-loop (reflecting) path appears, for example, in Proposition 3.7 of Boyd, Diaconis, Parrilo, and Xiao (2005). For Laplacian spectra of paths under other normalizations, see Van Mieghem (2023) or Brouwer and Haemers (2012).

B.2.1 *Production Networks: Cross-Section* With homogeneous labor shares, the Laplacian becomes $L = (1-\beta)I + \beta L_0$ and the eigenvalues are a convex combination of 1 and the eigenvalues of L_0 :

$$\lambda_i = (1-\beta) + \beta\Big(1 - \cos\Big(\frac{(i-1)\pi}{N}\Big)\Big), \qquad i = 1, \ldots, N.$$

This yields the results given in the text. Under heterogeneity, the Laplacian becomes $L = \mathrm{diag}(1-\beta_i+\beta) - \beta A_0$, which remains symmetric. While the spectrum is no longer a simple transform of L_0, it has simple structure. The smallest eigenvalue λ_1 satisfies: $L\overline{v} = \lambda_1 \overline{v}$, which for an interior mode means:

$$-\frac{\beta}{2}\overline{v}_{i-1} + d_i\overline{v}_i - \frac{\beta}{2}\overline{v}_{i+1} = \lambda_1\overline{v}_i \;\; \Rightarrow (d_i - \lambda_1)\overline{v}_i = \frac{\beta}{2}\left(\overline{v}_{i-1} + \overline{v}_{i+1}\right).$$

So when $d_i - \lambda_1$ is small, the worst-case input $\overline{v}_i$ tends to be large.

B.2.2 *Production Networks: Aggregate Output* Again, we focus on the heterogeneous labor share case here. Recall that we have defined the multiplier vector as $G_0 = L^{-1}1_N$, with elements g_i, so that $\|G\|_\infty = \|G_0\|_2$ and $\|G\|_2^2 = \frac{1}{2}\,1_N^\top G_0$. As in the previous section, the tridiagonal form of the network facilitates characterization. Here $LG_0 = 1_N$ becomes, for interior nodes:

$$-\frac{\beta}{2}g_{i-1} + d_i\,g_i - \frac{\beta}{2}g_{i+1} = 1 \quad \Rightarrow d_i\,g_i = 1 + \frac{\beta}{2}(g_{i-1} + g_{i+1}).$$

This illustrates the local spill-over mechanism. A node with low d_i (low labor share, slow local dissipation) carries a larger local multiplier g_i. Because interaction is local, this effect propagates to neighboring multipliers $g_{i\pm1}$ and then decays with distance along the path.

As in the cross-sectional case, aggregate amplification depends not only on the distribution of labor shares but where these sectors lie on the chain. The dashed lines in Figure 2 show the worst-case input for aggregate output. Recall that under homogeneity, the worst-case input is a uniform shock to all sectors. Heterogeneity now tilts the worst-case away from uniformity, and loads more heavily on the bottleneck sector and its neighbors. But since we focus now on the common aggregate component, the shocks are much less concentrated than in the cross-sectional case.

B.3 *Calculations from Section 5.2*

B.3.1 *Baseline* In this example, the spectrum of L depends only on the product of the weights $\beta_1\beta_2$, while the singular values, and hence the volatility and amplification of shocks, depends on β_1 and β_2 separately. The eigenvalues of L are $\lambda_i = 1 \pm \sqrt{\beta_1\beta_2}$, so the system is stable and the smallest eigenvalue is $1 - \sqrt{\beta_1\beta_2}$. But worst-case amplification is controlled by the singular values. In particular, from Theorem 4 we have:

$$\|G\|_\infty = \bar{\sigma}(L^{-1}) = \frac{1}{\min_i \sigma_i(L)}.$$

A direct calculation gives:

$$L^\top L = \begin{pmatrix} 1+\beta_2^2 & -(\beta_1+\beta_2) \\ -(\beta_1+\beta_2) & 1+\beta_1^2 \end{pmatrix}.$$

The squared singular values of L are the eigenvalues of $L^\top L$, so direct calculations yield:

$$\min_i \sigma_i(L) = \sigma_1(L) = \sqrt{\frac{(2+\beta_1^2+\beta_2^2) - \sqrt{(\beta_1^2-\beta_2^2)^2 + 4(\beta_1+\beta_2)^2}}{2}}.$$

When $\beta_1 = \beta_2$ this reduces to $\sigma_1(L) = 1-\beta_1$, as before. But now heterogeneity in sectoral input shares decreases the singular value $\sigma_1(L)$ and therefore increases the $\mathcal{H}_\infty$ norm. In particular, say we fix $\beta_1\beta_2$ but increase the divergence between β_1 and β_2. Then we fix the determinant of $L^\top L$ but increase its trace, and therefore decrease its smaller eigenvalue. When the sectors have different input intensities, the network becomes more fragile.

The worst-case input vector $\overline{v}$ is the corresponding right singular vector of L^{-1}, and hence left singular vector of L, which solves $LL^\top \overline{v} = \sigma_1^2(L)\overline{v}$. This vector can be written:

$$\overline{v} \propto \begin{pmatrix} \beta_1+\beta_2 \\ 1+\beta_1^2-\sigma_1^2(L) \end{pmatrix}.$$

The most-sensitive output pattern is the corresponding left singular vector of L^{-1}, which solves $L^\top L\,\overline{u} = \sigma_1^2(L)\overline{u}$. Given the structure here, these vectors are closely related. If we let $\Pi = 1_2 1_2^\top - \mathrm{I}$ denote the coordinate-swap matrix, a direct calculation shows:

$$LL^\top \;=\; \Pi\,(L^\top L)\,\Pi.$$

So left and right singular vectors are simple permutations of each other: $\overline{v} = \Pi\,\overline{u}$. When $\beta_1 \neq \beta_2$, L is non-normal and $\overline{v} \neq \overline{u}$, so the most damaging shock pattern and the most amplified output pattern do not coincide. In particular, if the most-damaging input is concentrated in node 1, then the most-sensitive output is concentrated in node 2.

We can be even more explicit here. Letting $\overline{v} = (\overline{v}_1, \overline{v}_2)^\top$, define $s \equiv \beta_1+\beta_2 > 0$ and $d \equiv \beta_2^2 - \beta_1^2$. Then from the expression above we have

$$\frac{\overline{v}_1}{\overline{v}_2} = \frac{\beta_1+\beta_2}{1+\beta_1^2-\sigma_1^2(L)} = \frac{2(\beta_1+\beta_2)}{\sqrt{d^2+4s^2}+\beta_1^2-\beta_2^2} = \frac{2s}{\sqrt{d^2+4s^2}-d},$$

where the second equality uses the expression for $\sigma_1^2(L)$. Then we have $\overline{v}_1/\overline{v}_2 > 1$ if:

$$2s > \sqrt{d^2+4s^2} - d \Leftrightarrow \sqrt{d^2+4s^2} < 2s+d \Leftrightarrow d^2+4s^2 < (2s+d)^2 = d^2+4s^2+4sd \Leftrightarrow 4sd > 0.$$

Thus $\overline{v}_1/\overline{v}_2 > 1$ if and only if $\beta_2 > \beta_1$.

For the $\mathcal{H}_2$ norm, we solve the Lyapunov equation from Theorem 2, which here is

$$LP + PL^\top = I.$$

In particular we can express its diagonal elements as:

$$P_{11} = \frac{\beta_1^2 - \beta_1\beta_2 + 2}{4(1-\beta_1\beta_2)}, \qquad P_{22} = \frac{\beta_2^2 - \beta_1\beta_2 + 2}{4(1-\beta_1\beta_2)}.$$

Then from Theorem 2, the squared $\mathcal{H}_2$ norm is:

$$\|G\|_2^2 = \mathrm{tr}(P) = \frac{(\beta_1-\beta_2)^2 + 4}{4(1-\beta_1\beta_2)}.$$

Here we see directly that for fixed product $\beta_1\beta_2$, as the divergence between β_1 and β_2 increases, output volatility as measured by the $\mathcal{H}_2$ norm increases.

B.3.2 *Static-neutral shocks* I work with the general case with weights (c_1, c_2). When $c_1 = c_2 = 1$, the results reduce to those in the text. The static aggregate exposure vector is $q = L^{-\top}c$. Since

$$L^{-1} = \frac{1}{1-\beta_1\beta_2}\begin{pmatrix} 1 & \beta_1 \\ \beta_2 & 1 \end{pmatrix},$$

we may ignore the common leading scalar and write $q_1 = c_1 + \beta_2 c_2$ and $q_2 = \beta_1 c_1 + c_2$. With two sectors, the static-neutral subspace is one-dimensional. An orthonormal basis vector is

$$B_{\mathcal{S}} = \frac{1}{\sqrt{q_1^2 + q_2^2}}\begin{pmatrix} q_2 \\ -q_1 \end{pmatrix}.$$

By a direct calculation, the static-neutral transfer function is therefore

$$G_{\mathcal{S}}(s) = \frac{(\beta_1 c_1^2 - \beta_2 c_2^2)s}{\sqrt{q_1^2+q_2^2}\left((1+s)^2 - \beta_1\beta_2\right)}.$$

Clearly $G_{\mathcal{S}}(0) = 0$, as required. But if $\beta_1 c_1^2 \neq \beta_2 c_2^2$ then $G_{\mathcal{S}}(s)$ is not identically zero, so static-neutral shocks generate aggregate fluctuations at nonzero frequencies.

Evaluating at $s = j\omega$, the frequency response is

$$|G_{\mathcal{S}}(j\omega)| = \frac{|\beta_1 c_1^2 - \beta_2 c_2^2|\,\omega}{\sqrt{q_1^2+q_2^2}\sqrt{(1-\beta_1\beta_2-\omega^2)^2 + 4\omega^2}}.$$

This is maximized at the interior frequency $\omega^* = \sqrt{1-\beta_1\beta_2}$, and the $\mathcal{H}_\infty$ norm is

$$\|G_{\mathcal{S}}\|_\infty = \frac{|\beta_1 c_1^2 - \beta_2 c_2^2|}{2\sqrt{q_1^2+q_2^2}}.$$

B.4 *General Directed Cycle*

The row-stochastic adjacency matrix A_0 shifts mass one step forward around the circle:

$$(A_0)_{i,i-1} = 1 \text{ for } i = 2,\ldots,N, \qquad (A_0)_{1N} = 1,$$

and $(A_0)_{ij} = 0$ otherwise. Thus A_0 is a circulant permutation matrix, hence unitary and therefore normal. Gray (2006) characterizes the spectrum of A_0 in terms of the discrete Fourier transform.[29] As before, let $j = \sqrt{-1}$, then define $\theta_i = \frac{2\pi(i-1)}{N}$ and $\zeta_i = e^{-j\theta_i}$ for $i = 1, \ldots, N$. Then the eigenvalues of A_0 are $\{\zeta_i\}$ and the eigenvalues of L_0 are

$$\lambda_i = 1 - \zeta_i = 1 - \cos\theta_i + j\sin\theta_i,$$

with corresponding eigenvectors:

$$v_i = \frac{1}{\sqrt{N}}\left(1, \zeta_i^{-1}, \zeta_i^{-2}, \ldots, \zeta_i^{-(N-1)}\right)^\top.$$

Hence we have

$$\Re(\lambda_i) = 1 - \cos\theta_i = 2\sin^2\left(\frac{\theta_i}{2}\right), \qquad \Im(\lambda_i) = \sin\theta_i.$$

As usual $\lambda_1 = 0$ corresponds to the consensus eigenvector 1_N, while the remaining eigenvalues appear in complex conjugate pairs.

B.4.1 *Production Networks: Cross-Section, Homogeneous Labor* With homogeneous labor shares the network Laplacian is again $L = (1-\beta)I + \beta L_0$, so its eigenvalues are

$$\lambda_i = 1 - \beta\zeta_i = 1 - \beta\cos\theta_i + j\beta\sin\theta_i,$$

where ζ_i and θ_i are as defined above. As always, the $\mathcal{H}_\infty$ norm reduces to $1/(1-\beta)$. Directedness does not move the worst-case away from frequency zero, and the dominant mode is still the uniform mode. For the $\mathcal{H}_2$ norm, (9) yields:

$$\|G\|_2^2 = \frac{1}{2}\sum_{i=1}^{N}\frac{1}{\Re(\lambda_i)} = \frac{1}{2}\sum_{i=1}^{N}\frac{1}{1-\beta\cos\theta_i}.$$

This admits a closed form. Let $r = \beta/(1+\sqrt{1-\beta^2})$. Then

$$\sum_{i=1}^{N}\frac{1}{1-\beta\cos\theta_i} = \frac{N}{\sqrt{1-\beta^2}}\cdot\frac{1+r^N}{1-r^N}.$$

Since $r^N \to 0$ with N, we have:

$$\|G\|_2^2 = \frac{N}{2\sqrt{1-\beta^2}}\cdot\frac{1+r^N}{1-r^N} \sim \frac{N}{2\sqrt{1-\beta^2}} \text{ as } N \to \infty.$$

Cross-sectional volatility is driven by the density of slowly damped long-wavelength modes. It scales linearly with the number of sectors even though no sector is central.

[29] See Section 3.1 and Theorem 3.1 of Gray (2006). Van Mieghem (2023) provides the related spectrum of an undirected cycle.

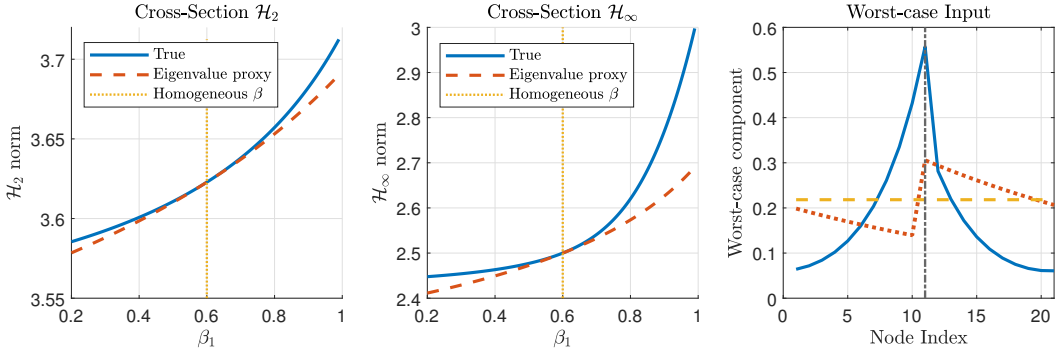


FIGURE B.1. The left and center panels plot the $\mathcal{H}_2$ and $\mathcal{H}_\infty$ norms for a 21-node directed cycle production network with cross-sectional output, where 20 sectors have share parameter $\beta = 0.6$ and one sector has β_1. Shown are the true values along with the normal proxies calculated using the Laplacian eigenvalues. The right panel plots the worst-case input vector $\overline{v}$ when $\beta_1 = 0.95$.

B.5 *Production Networks: Cross-Section, Heterogeneous Labor Shares*

Unlike the earlier examples, the dynamics are no longer normal with heterogeneous labor shares. Under heterogeneous labor shares, the Laplacian takes the form $L = D - \beta A_0$ with $D = \text{diag}(d_1, \ldots, d_N)$ and $d_i = 1 - \beta_i + \beta$. Such an L is no longer normal because while A_0 is normal it is not symmetric.[30] With heterogeneity, we need to consider the more general formulas (6) and (3), which depend on more than just the spectrum of L.

I consider a simple case of heterogeneity where, as in the path example above, $N-1$ sectors have a common intermediate share β, while one sector has a different share β_1. In Figure B.1, I set $N = 21$ and plot the $\mathcal{H}_2$ and $\mathcal{H}_\infty$ norms, fixing $\beta = 0.6$ and varying β_1. Shown are the true values of the norms, along with the normal proxies calculated using the Laplacian eigenvalues. When β_1 is close to β, the normal proxies are close to the true values. They diverge particularly when β_1 increases toward one and thus becomes a relative bottleneck, and especially in the worst-case.

The right panel shows the worst-case input vector $\overline{v}$ when $\beta_1 = 0.95$ at location $i = 11$. Here this is the right singular vector associated with the largest singular value of $G(0) = L^{-1}$. For comparison, the figure also shows the eigenvector associated with the eigenvalue of L with the smallest real part, which would be the worst-case input if the dynamics were normal. Relative to the homogeneous case, the worst-case input now loads very significantly on the bottleneck sector, with weights that decay with distance from it. Moreover, since upstream and downstream effects are now distinct, the input vector is asymmetric. For example node 10 feeds directly into the bottleneck sector, while node 12 must pass through the whole cycle before it hits the bottleneck. Thus the worst-case input weights decay more rapidly downstream of the bottleneck than they do upstream. Note as well that the normal-proxy eigenvector gives a quite different input pattern.

[30] Precisely, we have $LL^\top - L^\top L = \beta(DA_0 - A_0 D) + \beta(A_0^\top D - DA_0^\top)$. This vanishes only when A_0 commutes with D, which here requires $\beta_i = \beta$.

To understand these effects, it is helpful to see how this cycle network operates on a steady-state input. Letting $x = L^{-1}u$, then $Lx = u$ implies the componentwise equations for each $i = 1, \ldots, N$ (modulo N),

$$d_i x_i - \beta x_{i-1} = u_i.$$

Rearranging yields the one-step recursion

$$x_i = \frac{\beta}{d_i}\, x_{i-1} + \frac{1}{d_i}\, u_i.$$

A shock u_i hits x_i directly with gain $1/d_i$, while upstream activity x_{i-1} is transmitted forward to x_i with gain β/d_i. Hence a sector with a small labor share (high β_i, small d_i) amplifies both its own disturbance and the upstream state. The directed cycle propagates an asymmetric downstream "wake" in the cross-sectional response. This helps explain why the worst-case input shifts toward the bottleneck sector and is asymmetric around it.

With the recursion given in the text, we can solve explicitly for the aggregate output multipliers. Letting $h_i = 1/d_i$, unwinding one full lap around the cycle yields:

$$G_{0,i} = \frac{h_i + \beta h_i h_{i+1} + \beta^2 h_i h_{i+1} h_{i+2} + \cdots + \beta^{N-1} h_i h_{i+1} \cdots h_{i+N-1}}{1 - \beta^N \prod_{j=1}^{N} h_j},$$

with indices interpreted modulo N. The feedback term in the denominator captures the additional amplification from repeated laps.

Appendix C: Empirical Analysis

C.1 *Data Sources and Construction*

I use data from the U.S. Bureau of Economic Analysis (2026), generally following the construction of the benchmark networks used by Acemoglu, Carvalho, Ozdaglar, and Tahbaz-Salehi (2012), but adjusted for the revised data. In particular, I use the *Input-Output Accounts* and *Input-Output Interactive Data Tables*, especially the After Redefinitions and Underlying Detail Tables. For the finest level of disaggregation, I use the 2017 detailed benchmark input-output statistics, which is the most recent available.

The 2017 detailed after-redefinitions workbook reports a commodity-by-industry direct requirements matrix D, where D_{cj} is the direct share of commodity c used in producing one dollar of output by industry j. Because the model uses a square sector network, I retain the common BEA codes that appear both as commodity rows and industry columns, giving a square common-code direct requirements matrix D_S for 398 sectors. The four omitted industry columns lack same-code commodity rows in the direct-requirements table, while several row-only entries are BEA special commodity/accounting adjustments rather than industries. In the notation of the model, rows index producing sectors and columns index input-supplying sectors, so I use $A = D_S^\top$.

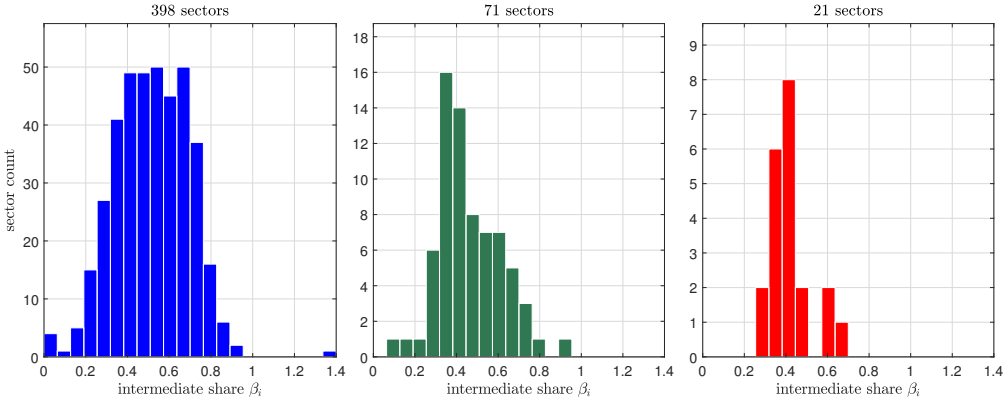


FIGURE C.1. Intermediate input share β_i in 2017 for different levels of aggregation.

The sector-specific intermediate-input share is therefore $\beta_i = \sum_j A_{ij}$, which is equivalently the column sum of the BEA direct-requirements table for industry i, restricted to the retained common-code inputs.

Figure C.1 illustrates the sectoral heterogeneity, showing the distribution of sectoral intermediate input shares β_i in 2017 at different levels of aggregation. At the full 398-sector level, the unweighted mean β_i is 0.516 with a standard deviation of 0.176, while at the 71-sector level the mean is 0.46 with a standard deviation of 0.152. At the detailed level one sector has $\beta_i > 1$, violating a stated condition for Theorem 4. However, the theorem is valid under the weaker condition $\rho(A) < 1$, which holds here.

For the annual time series I use the BEA after-redefinitions summary workbooks. These files provide annual commodity-by-industry direct requirements for a consistent 71-summary-industry panel from 1997 to 2023. I use the 71-sector panel and also construct broader panels using the BEA industry hierarchy. When I construct a coarser direct-requirements matrix, I aggregate implied transactions rather than averaging coefficients. Let $\mathcal{G}$ denote a partition of the fine industries into broader groups. For a supplier group $g \in \mathcal{G}$ and a buyer group $h \in \mathcal{G}$, the aggregated direct requirement is

$$D^{\mathcal{G}}_{gh} = \left(\sum_{i \in g} \sum_{j \in h} D_{ij} X_j \right) / \left(\sum_{j \in h} X_j \right),$$

where D_{ij} is the direct requirement of fine supplier i by fine buyer j, and X_j is gross output of fine buyer j. The numerator is the total dollar flow from suppliers in group g to buyers in group h, and the denominator is total gross output of buyers in group h. The model matrix is then $A^{\mathcal{G}} = (D^{\mathcal{G}})'$, so rows index producing sectors and columns index suppliers.

C.2 *Output Weights*

The state vector x_t in the model is the vector of sectoral log gross-output deviations. For the quantitative exercise, I map this vector into aggregate GDP. To construct the weight

vectors, gross output and value added are taken from the corresponding BEA make/use, transactions, or direct-requirements files from U.S. Bureau of Economic Analysis (2026).

Let $X_{i,t}$ denote gross output of industry i, and let $VA_{i,t}$ denote its value added. Aggregate GDP is the sum of industry value added,

$$Y_t \equiv GDP_t = \sum_{i=1}^{N} VA_{i,t}.$$

Log-linearizing around a reference point, with values $\overline{VA}_i$ and $\overline{Y}$, gives

$$d\log Y_t = \sum_{i=1}^{N} \frac{\overline{VA}_i}{\overline{Y}}\, d\log VA_{i,t}.$$

The state variable in the model is $x_{i,t} = d\log X_{i,t}$, rather than $d\log VA_{it}$. To connect gross output to value added, I use the local fixed-share approximation

$$VA_{it} \approx (1-\beta_i)X_{it},$$

where again β_i is the intermediate input share. Under this approximation,

$$d\log VA_{it} \approx d\log X_{it} = x_{it}.$$

Therefore a first-order approximation to aggregate GDP is

$$d\log GDP_t \approx \sum_{i=1}^{N} \nu_i x_{it}, \qquad \nu_i \equiv \frac{\overline{VA}_i}{\overline{GDP}}.$$

The aggregate-output calculations set $c = \nu$, so $y = \nu^\top x$ is approximately aggregate GDP.

This weighting is closely related to Domar weights commonly used in the networks literature, as in Acemoglu, Carvalho, Ozdaglar, and Tahbaz-Salehi (2012). In fact, if we let $\ell_i \equiv \overline{X}_i/\overline{GDP}$ denote the raw Domar weight, then $\nu_i = (1-\beta_i)\ell_i$. Hence value-added shares are Domar weights scaled by the non-intermediate share. Unlike raw Domar weights, the value-added shares sum to one, and so they provide the natural first-order weights for aggregating sectoral log gross-output deviations into log GDP deviations.[31]

For cross-sectional output, I use the same GDP weights to define a weighted Euclidean norm over sectoral responses. Specifically, I set $C = \mathrm{diag}(\sqrt{\nu})$. Then

$$\|Cx_t\|_2^2 = x_t^\top C^\top C x_t = x_t^\top \,\mathrm{diag}(\nu) x_t = \sum_{i=1}^{N} \nu_i x_{i,t}^2.$$

Thus the cross-sectional H_2 and H_∞ norms measure the GDP-share-weighted energy of sectoral output responses. This object gives greater weight to economically important sectors while avoiding cancellation between positive and negative sectoral movements.

[31] In their analysis, Acemoglu, Carvalho, Ozdaglar, and Tahbaz-Salehi (2012) assumed homogeneous input shares, so the GDP weights are proportional to Domar weights, $\nu = (1-\beta)\ell$. With heterogeneous shares, the weights differ, with Domar weights putting relatively more mass on intermediate-intensive sectors.

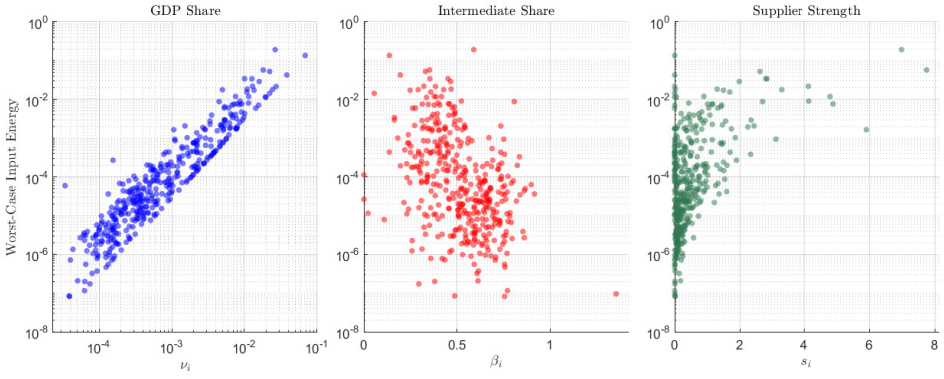


FIGURE C.2. Worst-case input energy for the 2017 detailed 398-sector network versus sectoral indicators: GDP share ν_i (left), intermediate share β_i (center), and supplier strength s_i (right).

C.3 *Sectoral Aggregation*

Figure C.2 shows scatter plots of the worst-case input energy for aggregate output in the 2017 detailed 398-sector network versus different sectoral indicators. The left panel shows that worst-case energy is highly correlated with the sector's GDP share ν_i, with a correlation of 0.74. The other panels show that the worst-case energy is weakly negatively correlated (-0.14) with the sector's intermediate share β_i (center), and weakly positively correlated (0.48) with the sector's supplier strength s_i (right).

Table C.1.: Aggregation breakdown from 71 sectors to coarser groupings

71-sector industry	49-group aggregation	32-group aggregation	21-sector aggregation
Farms	Primary goods	Agriculture, Forestry, Fishing, And Hunting	Agriculture, Forestry, Fishing, And Hunting
Forestry, fishing, and related activities	Primary goods	Agriculture, Forestry, Fishing, And Hunting	Agriculture, Forestry, Fishing, And Hunting
Oil and gas extraction	Primary goods	Mining	Mining
Mining, except oil and gas	Primary goods	Mining	Mining
Support activities for mining	Primary goods	Mining	Mining
Utilities	Utilities and construction	Utilities	Utilities
Construction	Utilities and construction	Construction	Construction
Wood products	Durable goods	Durable Goods	Durable Goods
Nonmetallic mineral products	Durable goods	Durable Goods	Durable Goods
Primary metals	Durable goods	Durable Goods	Durable Goods
Fabricated metal products	Durable goods	Durable Goods	Durable Goods
Machinery	Durable goods	Durable Goods	Durable Goods
Computer and electronic products	Durable goods	Durable Goods	Durable Goods
Electrical equipment, appliances	Durable goods	Durable Goods	Durable Goods
Motor vehicles, bodies, trailers, parts	Durable goods	Durable Goods	Durable Goods
Other transportation equipment	Durable goods	Durable Goods	Durable Goods
Furniture and related products	Durable goods	Durable Goods	Durable Goods
Miscellaneous manufacturing	Durable goods	Durable Goods	Durable Goods
Food, beverage, tobacco products	Nondurable goods	Nondurable Goods	Nondurable Goods
Textile mills and textile product mills	Nondurable goods	Nondurable Goods	Nondurable Goods
Apparel and leather products	Nondurable goods	Nondurable Goods	Nondurable Goods
Paper products	Nondurable goods	Nondurable Goods	Nondurable Goods
Printing and related support activities	Nondurable goods	Nondurable Goods	Nondurable Goods
Petroleum and coal products	Nondurable goods	Nondurable Goods	Nondurable Goods

Continued on next page

71-sector industry	49-group aggregation	32-group aggregation	21-sector aggregation
Chemical products	Nondurable goods	Nondurable Goods	Nondurable Goods
Plastics and rubber products	Nondurable goods	Nondurable Goods	Nondurable Goods
Wholesale trade	Wholesale trade	Wholesale trade	Wholesale Trade
Motor vehicle and parts dealers	Motor vehicle and parts dealers	Motor vehicles and parts retail	Retail Trade
Food and beverage stores	Food and beverage stores	Other retail	Retail Trade
General merchandise stores	General merchandise stores	Other retail	Retail Trade
Other retail	Other retail	Other retail	Retail Trade
Air transportation	Air transportation	Passenger transportation	Transportation And Warehousing
Rail transportation	Rail transportation	Freight transportation and storage	Transportation And Warehousing
Water transportation	Water transportation	Water and support transportation	Transportation And Warehousing
Truck transportation	Truck transportation	Freight transportation and storage	Transportation And Warehousing
Transit and ground passenger transportation	Transit and ground passenger transportation	Passenger transportation	Transportation And Warehousing
Pipeline transportation	Pipeline transportation	Freight transportation and storage	Transportation And Warehousing
Other transportation and support activities	Other transportation and support activities	Water and support transportation	Transportation And Warehousing
Warehousing and storage	Warehousing and storage	Freight transportation and storage	Transportation And Warehousing
Publishing industries, except internet	Publishing industries, except internet	Publishing and data services	Information
Motion picture and sound recording industries	Motion picture and sound recording industries	Media and telecommunications	Information
Broadcasting and telecommunications	Broadcasting and telecommunications	Media and telecommunications	Information
Data processing, internet publishing, and others	Data processing, internet publishing, and others	Publishing and data services	Information
Federal Reserve banks, credit intermediation, and related activities	Federal Reserve banks, credit intermediation	Core finance and insurance	Finance And Insurance
Securities, commodity contracts, and investments	Securities, commodity contracts, and investments	Core finance and insurance	Finance And Insurance
Insurance carriers and related activities	Insurance carriers and related activities	Core finance and insurance	Finance And Insurance
Funds, trusts, and other financial vehicles	Funds, trusts, and other financial vehicles	Funds and financial vehicles	Finance And Insurance
Housing	Housing	Housing and real estate	Real Estate And Rental And Leasing
Other real estate	Other real estate	Housing and real estate	Real Estate And Rental And Leasing
Rental and leasing services and lessors of intangible assets	Rental and leasing services and lessors	Rental and leasing	Real Estate And Rental And Leasing
Legal services	Legal services	Legal services	Professional And Technical Services
Computer systems design and related services	Computer systems design and related services	Computer and professional services	Professional And Technical Services
Miscellaneous professional, scientific, and technical services	Misc professional, scientific, and tech services	Computer and professional services	Professional And Technical Services
Management of companies and enterprises	Management of companies and enterprises	Management of companies and enterprises	Mgmt of Companies and Enterprises
Administrative and support services	Administrative and support services	Administrative and support services	Administrative And Waste Services
Waste management and remediation services	Waste management and remediation service	Waste management and remediation	Administrative And Waste Services
Educational services	Educational services	Educational services	Educational Services
Ambulatory health care services	Ambulatory health care services	Ambulatory health care	Health Care And Social Assistance
Hospitals	Hospitals	Hospitals and other health and social assistance	Health Care And Social Assistance

Continued on next page

71-sector industry	49-group aggregation	32-group aggregation	21-sector aggregation
Nursing and residential care facilities	Nursing and residential care facilities	Hospitals and other health and social assistance	Health Care And Social Assistance
Social assistance	Social assistance	Hospitals and other health and social assistance	Health Care And Social Assistance
Performing arts, spectator sports, museums, and related activities	Performing arts, spectator sports, museums	Arts, recreation, and gambling	Arts, Entertainment, And Recreation
Amusements, gambling, and recreation industries	Amusements, gambling, and recreation industries	Arts, recreation, and gambling	Arts, Entertainment, And Recreation
Accommodation	Accommodation	Accommodation and food services	Accommodation And Food Services
Food services and drinking places	Food services and drinking places	Accommodation and food services	Accommodation And Food Services
Other services, except government	Other services, except government	Other services, except government	Other Services, Except Government
Federal general government (defense)	Federal govt (defense)	Federal government	Government
Federal general government (nondefense)	Federal govt (nondefense)	Federal government	Government
Federal government enterprises	Federal government enterprises	Federal government enterprises	Government
State and local general government	State and local general government	State and local government	Government
State and local government enterprises	State and local government enterprises	State and local government	Government

For the aggregation exercises, I keep the 398-sector network as the underlying propagation system and use the BEA hierarchy to aggregate shock spaces to broader groupings. In between the BEA levels with 71 and 21 sectors, I add two intermediate levels with 49 and 32 groups which consider two different aggregation approaches. The groupings are detailed in Table C.1. The 49-group aggregation keeps almost all of the service sectors from the 71-sector level, but collapses the goods sectors even more than the 21-sector level. The 32-group aggregation collapses the services more, while keeping the goods sectors closer to the 21-sector partition. The 32-sector level is nested between 71 and 21, while the 49-sector level is distinct, motivated by the importance of service-sector industries in the network.

Consider a partition of the 398 sectors into K groups $\{g_1, \ldots, g_K\}$. The grouped-shock matrix B_K has one column for each group:

$$(B_K)_{i,j} = \frac{1\{i \in g_j\}}{\sqrt{n_{g_j}}}, \quad i = 1, \ldots 398, \quad j = 1, \ldots K,$$

where n_{g_j} is the number of sectors in group g_j. Thus $B_K^\top B_K = \mathrm{I}$, so each grouped shock direction has unit energy. Refining the partition enlarges the shock space without changing the overall power of the shocks.

Table C.2 provides the numerical values underlying Figure 5. The first row provides the norm values in the baseline 398-sector network, while the later rows show how much of those values are retained in coarser aggregations.

The $\mathcal{H}_2$ retention results also imply an orthogonal decomposition of aggregate-output variance in the detailed network. For an aggregation level with K groups, let $\mathcal{U}_K$ be the subspace of shocks that are constant within each group, and let $P_K = B_K B_K^\top$

TABLE C.2. 2017 detailed-network norm values and retention ratios

Case	Agg. $\mathcal{H}_\infty$	Agg. $\mathcal{H}_2$	Cross $\mathcal{H}_\infty$	Cross $\mathcal{H}_2$
398 baseline level	0.186	0.104	0.263	0.722
138 retention	0.985	0.988	0.999	0.873
71 retention	0.909	0.906	0.831	0.632
49 retention	0.900	0.901	0.830	0.612
32 retention	0.865	0.863	0.822	0.466
21 retention	0.768	0.754	0.629	0.356
15 retention	0.736	0.721	0.602	0.284
1 retention	0.462	0.439	0.332	0.064

be the Euclidean orthogonal projector onto $\mathcal{U}_K$. Let $G(s) = C(sI + L)^{-1}$ denote the full detailed-input transfer function, with $B = I_{398}$. Then the $\mathcal{H}_2$ norm at aggregation level K is $\|GB_K\|_2$. For a nested sequence of aggregation levels $\{0, 1, \ldots, M\}$,

$$\mathcal{U}_{K_0} \subset \mathcal{U}_{K_1} \subset \cdots \subset \mathcal{U}_{K_M} \subset \mathbb{R}^{398},$$

with $K_0 = 1$ denoting the pure aggregate shock and $P_{398} = I$, define

$$Q_{K_0} = P_{K_0}, \qquad Q_{K_\ell} = P_{K_\ell} - P_{K_{\ell-1}}, \quad \ell = 1, \ldots, M, \qquad Q_{398} = I - P_{K_M}.$$

These incremental projectors are mutually orthogonal and sum to I. Hence squared $\mathcal{H}_2$ norms decompose additively:

$$\|G\|_2^2 = \sum_{\ell=0}^{M} \|GQ_{K_\ell}\|_2^2 + \|GQ_{398}\|_2^2.$$

Thus, if $r_K = \|GB_K\|_2/\|G\|_2$ is the cumulative retention ratio at level K, the incremental variance share between adjacent levels is $s_{K_\ell} = r_{K_\ell}^2 - r_{K_{\ell-1}}^2$, with $s_{K_0} = r_{K_0}^2$ and residual detailed share $s_{398} = 1 - r_{K_M}^2$. From Table C.2, using the basic BEA nested sequence $1, 21, 71, 138, 398$, the resulting shares are: common aggregate shocks, 19.3%; 21-sector orthogonal to aggregate, 37.5%; 71-within-21 variation, 25.2%; 138-within-71 variation, 15.5%; and the remaining detailed residual, 2.5%.

C.4 *Time Series*

TABLE C.3. GDP-share weighted annual trend summary

	71-sector			21-sector		
Object	1997	2023	Change	1997	2023	Change
Aggregate $\mathcal{H}_\infty$	0.285	0.300	+5.2%	0.467	0.452	-3.2%
Aggregate $\mathcal{H}_2$	0.158	0.165	+4.5%	0.247	0.244	-1.1%
Cross $\mathcal{H}_\infty$	0.309	0.332	+7.5%	0.543	0.479	-11.9%
Cross $\mathcal{H}_2$	0.738	0.735	-0.5%	0.761	0.751	-1.3%

Table C.3 shows the main time-series comparison, which is illustrated in Figure 6. In the 71-sector panel, both aggregate and cross-sectional $\mathcal{H}_\infty$ increase over time, as does aggregate $\mathcal{H}_2$, while cross-sectional $\mathcal{H}_2$ is relatively flat. By comparison, for the more aggregated 21-sector network, aggregate $\mathcal{H}_\infty$ falls only mildly, and cross-sectional $\mathcal{H}_\infty$ falls more visibly. This suggests that aggregation may mask sources of volatility in the network, with reallocation within a broader sector masking fragility to finer shocks.

C.5 *Static-Neutral Shocks*

Table C.4 reports the leading sectors in the worst-case static-neutral input vector. Included are the real part of the loading, along with the energy share and the sector's GDP share. The time paths of the top five sectors are shown in Figure 8 in the text. The signs in the table use the normalization that the loading on housing is real and positive. Multiplying the vector by a common phase $e^{i\theta}$ only changes the time origin of $\Re(e^{i\omega t}v)$ and leaves the gain and energy shares unchanged. What matters is the relative phase pattern. Housing, state and local government, ambulatory health, construction, and retail move together, while other real estate, administrative support, insurance, chemicals, and primary metals load mainly in the opposite phase.

TABLE C.4. Leading components of the 2023 static-neutral peak input

Rank	Sector	Real loading	Energy	GDP
1	Housing	0.560	31.4%	9.4%
2	State and local general government	0.385	14.8%	6.5%
3	Other real estate	-0.342	11.7%	2.9%
4	Administrative and support services	-0.221	4.9%	2.9%
5	Ambulatory health care services	0.207	4.3%	3.6%
6	Insurance carriers and related activities	-0.200	4.2%	2.6%
7	Construction	0.201	4.0%	4.9%
8	Chemical products	-0.176	3.2%	1.7%
9	Other retail	0.172	3.0%	3.4%
10	Primary metals	-0.159	2.7%	0.3%